Coordination Chemistry Reviews 255 (2011) 2039–2057

Contents lists available at ScienceDirect

Coordination Chemistry Reviews

journal homepage: www.elsevier.com/locate/ccr

Review

Naked metal nanoparticles from metal carbonyls in ionic liquids: Easy synthesis and stabilization

Christian Vollmer, Christoph Janiak*

Institut für Anorganische Chemie und Strukturchemie, Heinrich-Heine-Universität Düsseldorf, Universitätsstrasse 1, D-40225 Düsseldorf, Germany

Contents

ARTICLE INFO

Article history:
Received 1 December 2010
Accepted 6 March 2011
Available online 16 March 2011

Keywords:
Metal nanoparticle
Ionic liquid
Metal carbonyl
Synthesis
Stabilization
Catalysis

ABSTRACT

An overview with more than 160 references on the synthesis and stabilization of metal nanoparticles (M-NPs) from metal carbonyls, metal salts in ionic liquids (ILs) and in particular from metal carbonyls in ionic liquids is given. The synthesis of M-NPs can proceed by chemical reduction, thermolysis, photochemical decomposition, electroreduction, microwave and sonochemical irradiation. Commercially available metal carbonyls $M_x(CO)_y$ are elegant precursors as they contain the metal atoms already in the zero-valent oxidation state needed for M-NPs. No extra reducing agent is necessary. The side product CO is largely given off to the gas phase and removed from the dispersion. The microwave induced thermal decomposition of metal carbonyls $M_x(CO)_y$ in ILs provides an especially rapid and energy-saving access to M-NPs because of the ILs significant absorption efficiency for microwave energy due to their high ionic charge, high polarity and high dielectric constant. The electrostatic and steric properties of ionic liquids allow for the stabilization of M-NPs without the need of additional stabilizers, surfactants or capping ligands and are highlighted by pointing to the DLVO (Derjaugin–Landau–Verwey–Overbeek) and extra-DLVO theory. Examples for the direct use of M-NP/IL dispersions in hydrogenation catalysis of cyclohexene and benzene are given.

1. Introduction

Metal nanoparticles (M-NPs) are of significant interest for technological applications in several areas of science and industry, especially in catalysis due to their high activity. The controlled and reproducible synthesis of defined and stable M-NPs with a small size distribution is very important for a range of applications [1–5]. Note that through the years metal nanoparticles were also referred to as nanophase metal clusters, metal nanocrystals and metal colloids. In the following we primarily use the term (metal) nanoparticles for simplicity. Small (< 5 nm) M-NPs are only kinetically stable and will combine to thermodynamically favored larger metal particles via agglomeration. This M-NP tendency for aggregation is due to the high surface energy and the large surface area. To avoid this agglomeration, M-NPs need to be stabilized with strongly coordinating protective ligand layers which provide electrostatic and/or steric protection like polymers and surfactants [6–8]. Ionic liquids (ILs) can be an alternative to such ligand layers (Scheme 1). ILs may be seen to act as a "novel nanosynthetic template" [9] that stabilize

* Corresponding author. Tel.: +49 211 81 12286.
E-mail address: janiak@uni-duesseldorf.de (C. Janiak).

0010-8545/$ – see front matter © 2011 Elsevier B.V. All rights reserved.
doi:10.1016/j.ccr.2011.03.005

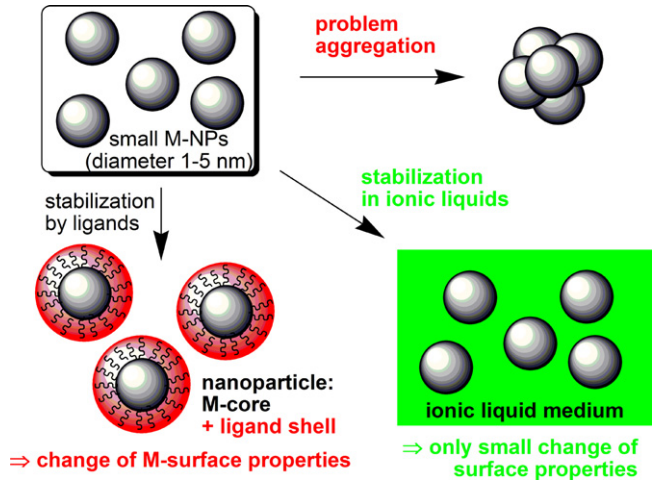

Scheme 1. Stabilization of metal nanoparticles (M-NP) through protective ligand stabilizers or in ionic liquids (IL). For the use of color in this graphic the reader is referred to the web version of the article.

M-NPs on the basis of their ionic nature [10], high polarity, high dielectric constant and supramolecular network (see Section 2) without the need of additional protective ligands (cf. Scheme 3) [11–15].

In the absence of strongly coordinating protective ligand layers, M-NPs in ILs should be effective catalysts. The IL network contains only weakly coordinating cations and anions (see Scheme 2) that bind less strongly to the metal surface and, hence, are less deactivating, than the commonly employed capping or protective ligands. The combination of M-NPs and ILs can be considered a *green catalytic system* because it can avoid the use of organic solvents. ILs are interesting in the context of green catalysis [16] which requires that catalysts be designed for easy product separation from the reaction products and multi-time efficient reuse/recycling [17–19]. Firstly, the very low vapor pressure of the IL and designable low miscibility of ILs with organic substrates allows for a facile separation of volatile products by distillation or removal in vacuum. Secondly, the IL is able to retain the M-NPs for catalyst reuse and recycling. For example, Dupont and coworkers recycled a M-NP/IL system quite easily and reused it several times without any significant changes in catalytic activity [11]. In recent reports of Rh- or Ru-NP/IL in hydrogenation reactions, the catalytic activity did not decrease upon repeated reuse [20,21]. A sizable number of catalytic reactions have successfully been carried out in ILs [22]. Generally, the catalytic properties (activity and selectivity) of dispersed M-NPs indicate

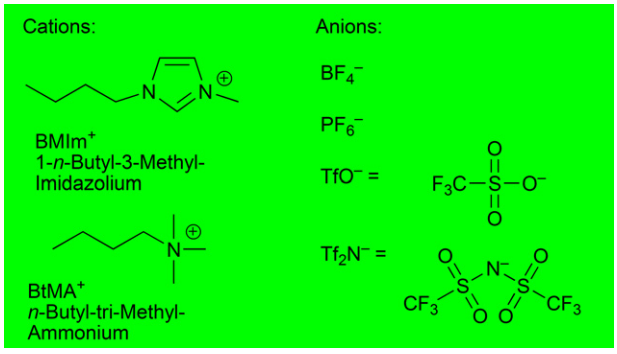

Scheme 2. Typical cations and anions of most common commercially available ILs. $BMIm^+$ is also abbreviated as BMI in the literature.

that they possess pronounced surface-like (multi-site) rather than single-site-like character [23,24].

In the following we give a brief introduction into the relevant properties of ionic liquids (Section 2) followed by an overview on the use of metal carbonyls for the synthesis of metal nanoparticles (Section 3). We then combine the synthesis of metal nanoparticles by various methods with ionic liquids as the matrix or medium for their preparation (Section 4). The theory for the treatment of particle dispersions, the DLVO (Derjaugin–Landau–Verwey–Overbeek) theory is then briefly discribed in Section 5.

2. Ionic liquids (ILs)

Ionic liquids are salts which are composed of charged inorganic and organic ion pairs. By definition their melting point is below 100 °C, more typically ILs are liquid at room temperature [18,25]. Such room temperature ionic liquids are occasionally abbreviated as RTILs [26]. ILs are liquid under standard ambient conditions because the liquid state is thermodynamically favorable, due to the large size and conformational flexibility of the ions involved, which leads to small lattice enthalpies and large entropy changes that favor melting [27]. ILs are characterized and set apart from other solvents by their physical properties like high charge density, high polarity, high dielectric constant and supramolecular network formation (Scheme 3) [14]. Typical IL cations include 1-alkyl-3-methylimidazolium, tetraalkylammonium, 1-alkylpyridinium and oxazolium. Typical anions for ILs are halide anions, tetrafluoroborate BF_4^-, hexafluorophosphate PF_6^-, tetrahalogenidoaluminate AlX_4^-, trifluoromethylsulfonate (triflate) $CF_3SO_3^-$ (TfO^-) or bis(trifluoromethylsulfonyl)amide [also named *N*-bis(trifluoromethanesulfonyl)imide, $(CF_3SO_2)_2N^-$, Tf_2N^-] (Scheme 2) [22,28].

The desired properties of the IL can be designed through judicious combination of anions and cations which presents an advantage over other solvent systems for the various envisioned IL applications. For instance: ILs containing Tf_2N^- offer low viscosity and high electrochemical and thermal stability [29]. If bis(*trifluoro*methylsulfonyl)amide Tf_2N^- is replaced by bis(methylsulfonyl)amide, viscosity increases and stability decreases [30]. This variety leads to a high interest towards ILs as new *green* reusable reaction media, especially in the field of catalysis [23].

Scattering experiments on ILs provided important information on the structure of ionic liquids which are not liquids in the conventional sense, but may rather be considered as mesophases [15]. Strictly speaking, however, ILs are not mesophases since they are isotropic liquids and just posses mesophases when they are liquid crystals. ILs are a class of substances that have an organizational behavior intermediate between isotropic liquids and liquid crystals. ILs have an intrinsic "nanostructure" which is caused by electrostatic, hydrogen bonding and van der Waals interactions [12,25]. The mesoscopic structure of imidazolium ionic liquids in particular can be described in part as a supramolecular three-dimensional hydrogen-bonded network (Scheme 3a) [12,14,15]. Pure 1,3-dialkylimidazolium ionic liquids can be described as a hydrogen-bonded [12,14,15] polymeric supramolecular network of the type $\{[(RR'Im)_x(A)_{x-n}]^{n+}[(RR'Im)_{x-n}(A)_x]^{n-}\}_n$ where RR′Im is the 1,3-dialkylimidazolium cation and A the anion. This structural pattern is not only seen in the solid phase but is also maintained to a great extent in the liquid phase. The introduction of other molecules and macromolecules proceeds with a disruption of the hydrogen bonding network and in some cases can generate nano-structures with polar and non-polar regions where inclusion-type compounds can be formed [11,12]. When mixed with other molecules or M-NPs, ILs

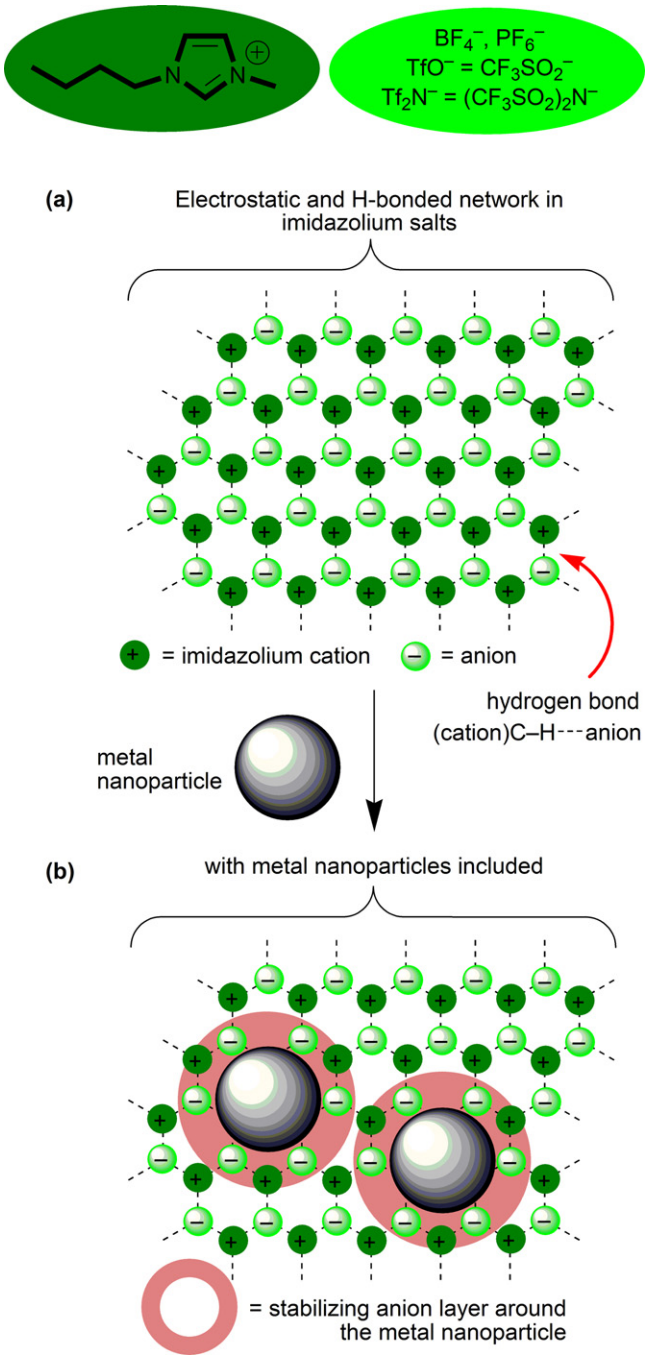

Scheme 3. (a) Schematic network structure in 1,3-dialkylimidazolium-based ionic liquids. (b) The inclusion of metal nanoparticles (M-NPs) in the supramolecular IL network with electrostatic and steric (=*electrosteric*) stabilization is indicated through the formation of the suggested primary anion layer forming around the M-NPs. For the use of color in this graphic the reader is referred to the web version of the article.

become nanostructured materials with polar and nonpolar regions [31–33].

Ionic liquids are nanostructural liquid media [34]. Nanometer-scale structuring in room-temperature ILs was observed by molecular simulation for ionic liquids belonging to the 1-alkyl-3-methylimidazolium family with hexafluorophosphate or with bis(trifluoromethylsulfonyl)amide as the anions. For ionic liquids with alkyl side chains longer than or equal to C_4, aggregation of the alkyl chains in nonpolar domains was observed. These domains permeate a three-dimensional network of charged or polar ionic channels formed by anions and by the imidazolium rings of the cations (cf. Scheme 3(a)). As the length of the alkyl chain increases, the nonpolar domains become larger and more connected and cause swelling of the ionic network, in a manner analogous to systems exhibiting microphase separation [34]. In other words, ILs are nanostructurally organized with nonpolar regions arising from clustering of the alkyl chains and ionic networks arising from charge ordering of the anions and imidazolium rings of the cations [26]. The combination of undirected Coulomb forces and directed hydrogen bonds leads to a high attraction of the IL building units. This is the basis for their (high) viscosity, negligible vapor pressure and three-dimensional constitution. The IL network properties should be well suited for the synthesis of defined nano-scaled metal colloid structures (see Scheme 3) [11–13].

3. Synthesis of metal nanoparticles (M-NPs) from metal carbonyls

The use of binary metal carbonyls for the synthesis of metal nanoparticles is sensible and logical. Metal carbonyls are commercially available (Table 1). $Fe(CO)_5$ and $Ni(CO)_4$ are industrially produced on a multi-ton scale [35]. Compounds $M_x(CO)_y$ are easily purifyable and handable, even if care should be exerted for the possible liberation of poisonous CO. The metal carbonyls contain the metal atoms already in the zero-valent oxidation state needed for M-NPs. No reducing agent is necessary. The side product CO is largely given off to the gas phase and removed from the dispersion. Contamination from by- or decomposition products, which are otherwise generated during the M-NP synthesis (see Section 4), are greatly reduced. Thus, metal carbonyls were used early on for the preparation of M-NPs. It will be evident from the following examples (see also Table 2) that all these metal nanoparticles which were prepared in the condensed phase needed stabilization through additional ligands, like dispersants, surfactants or through passivation with a metal-oxide shell. Also the majority of the work uses the metal carbonyls $Fe(CO)_5$ and $Co_2(CO)_8$. The following excerpts from the literature are roughly arranged in chronological order according to the year of publication (see also Table 2 for further examples). Much of the work on Fe- or Co-NPs at large is devoted to their magnetism [36].

In early reports Hess and Parker [37] and Thomas [38] described processes for preparing metallic cobalt particles of uniform size in the 10–1000 Å range (0.1–100 nm). Dicobalt octacarbonyl $Co_2(CO)_8$ was thermally decomposed in typically toluene solutions of dispersant polymers, such as methyl methacrylate-ethyl acrylate-vinylpyrrolidone terpolymers, high-purity polystyrene, styrene-acrylonitrile polymers, polyacrylonitril, chloropolyethylene sulfonamide, polyester and polyether urethanes to form stable colloids of discrete particles which are separated by polymer coatings. Variation of polymer composition, molecular weight and solvent result in a variation of particle size and colloid stability. Preparation of single-domain ferromagnetic cobalt particles with good magnetic properties was possible through a balance between dispersant polymer, solvent, and the growing metal particle [37].

Papirer et al. prepared a stable suspension of metallic cobalt particles in an organic solvent (ferrofluid) by decomposition of $Co_2(CO)_8$ [39,40]. The cobalt particles originate from the thermolysis of the dicobalt octacarbonyl solution in the presence of a chosen surface active agent. The reaction temperature, the nature of the solvent and of the surfactant, the weight ratio of carbonyl and surfactant, and the initial concentration of the cobalt carbonyl solution were varied. Spherical particles, of a narrow size distribution, are obtained when the decomposition of $Co_2(CO)_8$ is carried out in an aromatic solvent above 110 °C and in the presence of a sur-

Table 1
Binary metal carbonyls.[a]

Group Metal	5 V, Nb, Ta	6 Cr, Mo, W	7 Mn, Tc, Re	8 Fe, Ru, Os	9 Co, Rh, Ir	10 Ni, Pd, Pt
Mononuclear complexes	$V(CO)_6$	**$Cr(CO)_6$** **$Mo(CO)_6$** **$W(CO)_6$**		**$Fe(CO)_5$** $Ru(CO)_5$ $Os(CO)_5$		**$Ni(CO)_4$**
Polynuclear complexes			**$Mn_2(CO)_{10}$** $Tc_2(CO)_{10}$ **$Re_2(CO)_{10}$**	**$Fe_2(CO)_9$** **$Fe_3(CO)_{12}$** $Ru_2(CO)_9$ **$Ru_3(CO)_{12}$** $Os_2(CO)_9$ **$Os_3(CO)_{12}$**	**$Co_2(CO)_8$** **$Co_4(CO)_{12}$** **$Rh_4(CO)_{12}$** **$Rh_6(CO)_{16}$** **$Ir_4(CO_{12})$**	

[a] Metal carbonyls given in bold were confirmed to be commercially available, e.g., from Aldrich, ABCR or Acros.

factant possessing a long hydrocarbon chain and a strong ionic group (sulfonate). The decomposition in toluene, in which ethyl (2-hexyl) sodium sulfo-succinate is dissolved, leads to particles of about 70 Å in diameter. When a ferrofluid is being formed, an initial and rapid evolution of CO corresponding to the formation of $Co_4(CO)_{12}$ is recorded. Part of this compound is insoluble in the reaction medium and appears to be a regulating intermediate. After this short initial stage the rate of decomposition of $Co_4(CO)_{12}$ slows down and becomes practically constant. Later the CO formation is accelerated again and finally it decreases as the reaction goes to completion. This S-shaped curve which describes the decomposition of $Co_2(CO)_8$ is always observed when a ferrofluid is in progress of formation [39]. The diameters of the particles, and the number of growing particles have been measured using also small-angle X-ray scattering and magnetic methods. The presence of microreactors in the reaction medium and a diffusion controlled growth mechanism are seen as the responsible two factors for the formation of particles of very narrow size distribution [40].

Lee et al. produced nanoparticles of iron, chromium, molybdenum and tungsten by laser decomposition of the corresponding metal carbonyls with a 10.6 μm CO_2 laser in the presence of Ar and SF_6 [41]. Argon helped to increase the purity of the metal clusters by suppressing the formation of $(M)_x(CO)_y$ for M = Fe, Cr, Mo, W. SF_6 acted as an infrared photosensitizer, which initially absorbed the 10.6 μm IR photons from the CO_2 laser and transferred its energy to a metal carbonyl via collisions. The M-NP size distributions were narrow and the average diameter was 6, 3.5, 2 and ~1 nm for Fe, Cr, Mo and W clusters, respectively, as determined by TEM. The structure is body-centered cubic (bcc) for both Fe and Cr clusters, face-centered cubic (fcc) for Mo clusters, and amorphous for W clusters as determined from the X-ray diffraction patterns (note that all the bulk metals have bcc structure). The cluster size (n) in one cluster of average diameter was estimated by assuming a spherical shape such that n = (cluster volume/atomic volume) × packing fraction = $(r/r_0)^3 f$, with r the cluster radius, r_0 the atomic radius and f the packing fraction (0.68 for bcc and 0.74 for fcc). Considering the cluster sizes (n = 9630, 1870, 230 and ~30 for Fe-, Cr-, Mo- and W-NPs, respectively) estimated from their average diameters, it was found likely that there exists a structural transition from fcc to bulk bcc with increasing cluster size in these metal clusters [41].

Giersig and Hilgendorff prepared cobalt nanoparticles by thermolysis of $Co_2(CO)_8$ in Ar-saturated toluene as an organic carrier at 110 °C in the presence of two different surfactants. The surfactants

Table 2
Additional examples for M-NP syntheses from metal carbonyls.

Metal	Metal carbonyl	Solvent	M-NP size: range or average diameter (standard deviation) [nm]	Remarks, stabilizer	Reference
Fe	$Fe(CO)_5$	Octanol or hexadecane	3–8 (amorphous)	Sonochemical decomposition; stabilized by polyvinylpyrrolidone (PVP) or oleic acid	[75]
Fe	$Fe(CO)_5$	Trioctylphosphine oxide (TOPO)	2 (monodisperse, spherical)	Thermal decomposition, rod-shaped particles stabilized by TOPO; rod-shaped Fe-NPs from the controlled growth of the monodisperse spherical NPs	[76]
Fe	$Fe(CO)_5$	Decalin	2–10 (variation by the $Fe(CO)_5$/PIB ratio)	Stabilized by modified polyisobutylene (PIB); NP characterization also by magnetic measurements (fastoxidation in air); linear structures of the larger particles (by cryo-TEM) because of magnetic interaction	[77]
Co	$Co_2(CO)_8$	Toluene or THF	3–5	Thermal decompostition, stabilized by polystyrene(PS)-poly-4-vinyl-pyridine (PVP)	[78]
Co	$Co_2(CO)_8$	Trioctylphosphine oxide	20	Thermal decomposition, stabilized by TOPO; new structure of elemental cobalt (ε-cobalt)	[79]
$CoPt_3$	$Co_2(CO)_8$, $Pt(hfac)_2$	Hot toluene or nonane	1.8(1)	Thermal decomposition, stabilized by oleic acid or dodecane isocyanide; alloy nanoparticles	[80]
FeCo	$Co_2(CO)_8$, $Fe(CO)_5$	1,2-Dichlorobenzene	1–11	FeCo-alloyed nanoparticles, thermal decomposition, stabilized by oleic acid and trioctyl-phosphane oxide	[81,82]

used were sodium bis 2-(ethyl-hexyl)sulfosuccinate and oleoyl-sarcosine. The magnetic nanoparticles were then ordered into a two-dimensional array using a magnetophoretic technique. The quality of the ordering was observed by electron microscopy and the lattice constants determined by electron diffraction. Cobalt particles condense into a hexagonal close packed array [42]. These arrays of monodisperse colloidal 11.4 nm Co nanoparticles were investigated by multifrequency ferromagnetic resonance and X-ray magnetic circular dichroism (XMCD) to determine the ratio of orbital-to-spin magnetic moment as $\mu_L/\mu_S^{eff} = 0.24 \pm 0.06$ by XMCD [43].

Van Wonterghem, Mørup et al. [44,45], Pathmamanoharan et al. [46], Gossens et al. [47] and Butter, Philipse et al. [48] formed iron nanoparticles by thermolysis of $Fe(CO)_5$ in decalin with modified polyisobutene and oleic acid as stabilizers. The magnetic Fe-NPs are fairly monodisperse even for particle radii below 10 nm. The particle size can be increased by seeded growth, and the particle shape can be changed by using a mercaptan stabilizer, which leads to rod-like iron colloids. The thermal decomposition of iron pentacarbonyl in a mixture of decalin and sarkosyl-O (*n*-oleyoyl sarcosine) has been studied by Moessbauer spectroscopy. With the X-ray diffraction it was shown that the sample contained small particles of a metallic glass (amorphous material). Annealing of the particles at 523 K resulted in crystallization of the particles into a mixture of α-Fe and Fe_5C_2 [44]. Fe^{2+} was found in all samples. After some time of reaction, a new iron carbonyl complex appeared. During the final stages of the reaction, this intermediate carbonyl complex decomposed, and ultrafine particles of an amorphous $Fe_{100-x}C_x$ alloy were formed [45]. Moessbauer spectroscopy also showed that the Fe-NPs with $r = 5.3$, 6.9 and 8.2 nm are dominated by the broadened sextuplet with $H_{eff} = 262$ kOe similar to that found in the sarcosyl and oleic acid stabilized colloids. This hyperfine field characterizes $Fe_{1-x}C_x$ species with $x \approx 0.25$ by comparison with sputtered amorphous $Fe_{1-x}C_x$ films [49]. In addition, a small contribution of a sextuplet with $H_{eff} = 496$ kOe characterizing an Fe(III) oxidic contribution is visible in the spectra of the Fe-NPs with $r = 5.3$ and 6.9 nm. This Fe(III) oxidic contribution is absent for the largest NP with $r = 8.2$ nm, while the spectrum of the NPs with the smallest radius ($r = 2.1$ nm) turned out to be completely oxidic [47].

Huh et al. combined a thermal decomposition of metal carbonyls with a collision induced clustering. Metal carbonyls $Fe(CO)_5$ and $Mo(CO)_6$ were thermally decomposed with a hot filament and the resultant bare metal atoms underwent collisions to produce high purity Fe, Mo, and alloy Fe/Mo nanometer size metal particles [50].

By thermal decomposition of $Fe(CO)_5$ with simultaneous reduction of platinum acetylacetonate $Pt(acac)_2$ in the presence of oleic acid and oleyl amine Sun, Murray et al. synthesized monodisperse iron–platinum nanoparticles [51]. Chen and Nikles used this procedure for the preparation of FePd and FeCoPt alloy nanoparticles with very narrow size distribution, using $Fe(CO)_5$, $Pd(acac)_2$ or $Pt(acac)_2$ and $Co(acac)_2$ [52,53].

Puntes et al. reported the synthesis of monodisperse ε-Co nanoparticles with spherical shapes and sizes ranging from 3 to 17 nm by the rapid pyrolysis of a dicobalt octacarbonyl solution in dichlorobenzene in the presence of a surfactant mixture composed of oleic acid, lauric acid and trioctylphosphine. The size distribution and the shape of the nanocrystals were controlled by varying the surfactant (oleic acid, phosphonic oxides and acids, etc.) its concentration, and the reaction temperature [54].

Hyeon et al. utilized a high-temperature (300 °C) aging of an iron-oleic acid metal complex, which was in turn prepared by the thermal decomposition of iron pentacarbonyl in the presence of oleic acid at 100 °C to generate monodisperse iron nanoparticles. The Fe-NP particle size ranged from 4 to 20 nm. The resulting iron nanoparticles were then transformed to monodisperse γ-Fe_2O_3 nanocrystallites by controlled oxidation using trimethylamine oxide as a mild oxidant [55]. With a similar procedure Kim, Hyeon et al. prepared cobalt nanoparticles from $Co_2(CO)_8$, oleic acid, trioctylphosphine and dioctyl ether under reflux. The Co-NPs were applied as recyclable catalysts for Pauson–Khand reactions, which involve the cycloaddition of alkynes, alkenes and carbon monoxide to cyclopentenones [56].

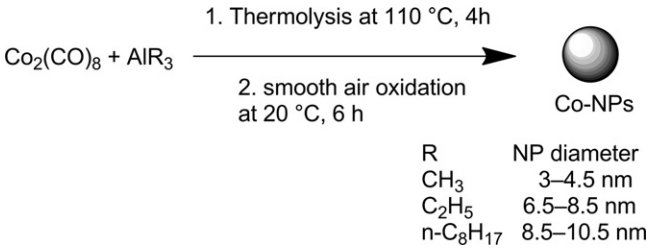

Scheme 4. Thermolysis of $Co_2(CO)_8$ in the presence of aluminium alkyls to Co-NPs and smooth air oxidation for surface passivation.

Burke et al. prepared polymer-coated iron nanoparticles by the thermal decomposition of $Fe(CO)_5$ in the presence of ammonia and polymeric dispersants [57]. The dispersants consist of polyisobutylene (PIB), polyethylene, or polystyrene chains functionalized with tetraethylenepentamine, a short polyethyleneimine chain. Inorganic-organic core–shell nanoparticles were formed with all three types of dispersants. With the PIB dispersants, the particle size is determined, in part, by the iron pentacarbonyl loading, increasing from 8 ± 1 nm for a 1:1 $Fe(CO)_5$/dispersant ratio to 20 ± 4 nm for a 5.5:1 ratio [57].

Rutnakornpituk et al. use copolymers as micelles in toluene to serve as nanoreactors for the thermal decomposition of $Co_2(CO)_8$ to superparamagnetic Co-NP dispersions. The steric stabilizers are poly[dimethylsiloxane-*b*-(3-cyanopropyl)methylsiloxane-*b*-dimethylsiloxane] (PDMS-PCPMS-PDMS) triblock copolymers in poly(dimethylsiloxane) carrier fluids. The nitrile groups on the PCPMS central blocks are thought to adsorb onto the particle surface. The Co-NP size could be controlled by adjusting the Co-to-copolymer ratio. TEM showed non-aggregated Co-NPs with narrow size distributions and evenly surrounded by the copolymer sheaths [58].

Diana et al. synthesized cobalt nanoparticles within inverse micelles of polystyrene-*block*-poly(2-vinylpyridine) copolymer in toluene by the pyrolysis of $Co_2(CO)_8$ at 115 °C [59]. The nanoparticle structure at different reaction times was investigated using transmission electron microscopy and Fourier transform infrared spectroscopy (FT-IR). At early reaction stages, the nanoparticles were noncrystalline from TEM; and FT-IR showed that the precursor was only partially decomposed. After 15 min of reaction, the nanoparticles became crystalline, forming chains due to magnetic interactions. The noncrystalline nanoparticles could be crystallized upon heating to 420 °C on grids in the transmission electron microscope. This produced nearly monodisperse single nanocrystals inside each micelle, with limited aggregation, but such annealing led to the degradation of the polymer [59].

Bönnemann et al. obtained monodisperse Co, Fe, and FeCo nanoparticles through thermal decomposition of the metal carbonyls $Co_2(CO)_8$, $Fe(CO)_5$ or $Fe(CO)_5/Co_2(CO)_8$ in the presence of aluminium alkyls (AlR_3), as air-stable magnetic metal nanoparticles after surface passivation [60–63]. After decomposition the metal particles were treated with synthetic air through a thin capillary (*smooth oxidation*) (Scheme 4) to yield particles stable in air under ambient conditions for over 1 year, as confirmed by magnetic measurements.

The aluminium alkyl acts as a catalyst, activating the thermal decomposition of the metal carbonyl as well as the surface

passivation during the *smooth oxidation*. The resulting particles strongly depend on the alkyl chain length *R* of the aluminium alkyl and the $Co_2(CO)_8$ to AlR_3 ratio. Monodisperse Co nanoparticles, 3–4.5, 6.5–8.5 and 8.5–10.5 nm in diameter, were obtained for $Al(CH_3)_3$, $Al(C_2H_5)_3$ and $Al(C_8H_{17})_3$, respectively. The particles were characterized by electron microscopy (SEM, TEM), electron spectroscopy (MIES, UPS, and XPS) and X-ray absorption spectroscopy (EXAFS). EXAFS measurements showed that this preparation pathway provides long-term stable zerovalent magnetic cobalt particles [62]. The chemical nature of the surfactant used exerts a significant influence on the stability and the local electronic and geometric structure of the analyzed nanoparticles [61]. With the help of surfactants, for instance oleic acid or cashew nut shell liquid, the metal particles can be peptized in organic solvents like toluene or kerosene, resulting in magnetic fluids. The saturation of magnetization, *Ms*, of the fluids was determined by specific magnetization. The sizes and structure of the particles were investigated by transmission electron microscopy, and Moessbauer analysis showed that the core of the particles was metallic or alloyed, respectively. The particle surface termination was studied by X-ray photoelectron and Auger electron spectroscopy [61]. The particles were also peptized by surfactants to form stable magnetic fluids in various organic media and water, exhibiting a high volume concentration and a high saturation magnetization. In view of potential biomedical applications of the particles, several procedures for surface modification are possible, including peptization by functional organic molecules, silanization, and *in situ* polymerization [62]. Other procedures for surface modification of these pre-stabilized, metallic Co-NPs include direct anchoring of surface-active functional groups and biocompatible dextran layers as well as silica and polymer coatings. As a result, individually coated nanoparticles as well as microspheres can be obtained [63].

Yin et al. (2004) formed a Pt@CoO yolk–shell nanostructure in which a platinum nanocrystal of a few nanometers was encapsulated in a CoO shell [64]. This was achieved by first reducing platinum acetylacetonate with a longchain polyol to form uniform platinum nanoparticles in the presence of surfactants such as oleic acid, oleylamine, and trioctylphosphine. The size of the platinum particles was tuned from 1 to 10 nm, depending on the concentration of surfactants. $Co_2(CO)_8$ was then injected into the hot solution and decomposed to form a conformal coating on the platinum nanocrystals. Oxidation of the Pt@Co nanocrystals was performed a few minutes after introduction of the cobalt carbonyl by blowing a stream of O_2/Ar mixture into the colloidal solution at 455 K [64].

Zubris et al. describe the synthesis of iron and cobalt alloy nanoparticles by the co-decomposition of iron and cobalt carbonyl precursors in the presence of polystyrene as a surface stabilizing agent [65]. The decomposition kinetics of $Fe(CO)_5$ and $Co_2(CO)_8$ were established and controlled. The results suggest that $Fe(CO)_5$ decomposition is a higher-order process (not first-order as previously assumed), with a complicated intermediate mechanism. Equal initial concentrations of both precursors generated nanoalloys with a crystalline core–shell dense morphology, while precursor concentrations corresponding to initial equal rates of decomposition generated polycrystalline nanoalloys with a diffuse morphology [65].

Korth et al. synthesized polystyrene (PS)-coated cobalt nanoparticles by the thermolysis of $Co_2(CO)_8$ in the presence of end-functional polymeric surfactants in refluxing 1,2-dichlorobenzene [66]. A mixture of amine and phosphine oxide PS surfactants (4:1 wt ratio) was used in the thermolysis of $Co_2(CO)_8$ to prepare polymer-coated cobalt nanoparticles, where the ligating end group passivated the colloidal surface. The combination of both amine and phosphine oxide ligands on the PS chain was necessary to yield uniform ferromagnetic nanoparticles. These polymer-coated cobalt nanoparticles (PS-Co) were then characterized using TEM, atomic force microscopy (AFM), and magnetic force microscopy (MFM) to determine particle size and morphology of magnetic colloids and nanoparticle chains [66].

It is obvious that the use of metal carbonyls for M-NP preparation will also be noted in the patent literature. An example is given by Mercuri, describing "a process for producing nano-scale metal particles which includes feeding at least one metal carbonyl into a reactor vessel; exposing the metal carbonyl to a source of energy sufficient to decompose the metal carbonyl to produce nano-scale metal particles; and depositing or collecting the metal nanoparticles. Oxygen is fed into the reactor vessel to partially oxidize the nanoscale metal particles produced by decomposition of the decomposable moiety. The nanoscale metal particles are then brought onto an end-use substrate which are intended to be employed, such as the aluminium oxide or other components of an automotive catalytic converter, or the electrode or membrane of a fuel cell or electrolysis cell" [67,68].

Gergely et al. describe "a process for preparing superparamagnetic transition metal nanoparticles by introducing into a gas stream a hydrocarbon and a transition metal carboxyl wherein the transition metal carbonyl is introduced downstream from the hydrocarbon; wherein at the point of introduction of the hydrocarbon the gas stream is as a plasma, and wherein at the point of introduction of the transition metal carbonyl the gas stream is at a temperature of at least 1000 °C, followed by quenching to form C-coated transition metal nanoparticles; and wherein the gas stream consists essentially of at least one inert gas and H" [69].

Gürler et al. showed that hydroxyfunctional cobalt nanoparticles can be obtained in a single step by thermal decomposition of $Co_2(CO)_8$ in the presence of ricinolic acid as a functional surfactant. The chemisorbed ricinolic acid through the carboxylic acid group served to introduce hydroxyl groups that serve as an initiator for the ring-opening polymerization of 3-caprolactone to give the desired hybrid cobalt/polycaprolactone brush particles [70].

Doan et al. investigated the oxidation of Co nanoparticles stabilized with various ligands in an autoclave [71]. Tridodecylamine stabilized Co nanoparticles with different sizes (8, 22 and 36 nm) were prepared by thermal decomposition of $Co_2(CO)_8$ in dodecane. The oxidation of the particles was studied by introducing oxygen into the autoclave and following the oxygen consumption with a pressure meter. Tridodecylamine capped particles were initially oxidized at a high rate, however, the oxidation layer quickly inhibited further oxidation. The thickness of the oxide layer estimated from the oxygen consumption was 0.8 nm for all three particle sizes showing that the oxidation is size independent in the studied particle size range. The tridodecylamine ligand was exchanged for various long chain carboxylic acids followed by subsequent oxidation. With the carboxylic acids the formed oxide layer does not inhibit further oxidation as effectively as in the case of tridodecylamine. TEM studies show that tridodecylamine capping leads to particles with a metal core surrounded by an oxide layer, while particles capped with long chain carboxylic acids form hollow cobalt oxide shells [71].

Howard and coworkers used a carbonyl metallate $Na_2Fe(CO)_4$ (Collman's reagent) and $Pt(acac)_2$ to synthesize bimetallic fcc and face-centered tetragonal (fct) FePt nanoparticles in hydrocarbon solvents with the size of 3 nm stabilized by oleic acid [72].

Another way to generate bimetallic FePt nanoparticles is the decomposition of the bimetallic cluster $Pt_3Fe_3(CO)_{15}$ by sonication in toluene, oleic acid and oleylamine. The resulting nanoparticles had a size of 2 nm [73].

Robinson et al. used the bimetallic carbonyl metallate cluster anions $[FeCo_3(CO)_{12}]^-$, $[Fe_3Pt_3(CO)_{15}]^{2-}$, $[FeNi_5(CO)_{13}]^{2-}$ and $[Fe_4Pt(CO)_{16}]^{2-}$ as precursors and obtained the bimetallic $FeCo_3$, FePt, $FeNi_5$ and Fe_4Pt, respectively, particles by thermal decompo-

sition in 1,2-dichlorobenzene with the average diameters of 7.0, 4.4, 2.6 and 3.2 nm, respectively. The size variation is due to the use of different stabilizers like oleic acid, myristic acid or hexadecyl amine [74].

The aforementioned examples together with reviews on the chemical synthesis of metal nanoparticles [36] illustrate the wide applicability of commercial $Fe(CO)_5$ and $Co_2(CO)_8$ for the preparation of iron- and cobalt-containing nanoparticles (additional examples are given in Table 2). Yet, it is also evident that the utilization of metal carbonyls in nanoparticle synthesis is largely limited to these two carbonyl compounds. This may in part be due to the strong interest in magnetic M-NPs. It also becomes clear that the prepared M-NPs need a protecting layer to prevent aggregation to larger particles or oxidation.

4. Synthesis of metal nanoparticles (M-NPs) in ionic liquids (ILs)

Metal nanoparticles can be synthesized in ionic liquids [83] through chemical reduction [21,84–89] or decomposition [90–93], by means of photochemical reduction [94,95] or electro-reduction [96–98] of metal salts where the metal atom is in a formally positive oxidation state and by decomposition of metal carbonyls with zero-valent metal atoms [9,20,21,99] without the need of extra stabilizing molecules or organic solvents [6,11,13,100,101].

A myriad of M-NPs have been prepared in ILs from compounds with the metal in a formally positive oxidation state M^{n+}. Such M-NPs then include, for example, the main-group metals and metalloids Al [102], Te [103], and the transition metals Ru [104], Rh [87], Ir [105], Pt [106], Ag [84,107], Au [108] (cf. Table 3).

The inclusion of metal nanoparticles in the supramolecular ionic liquid network brings with it the needed electrostatic and steric (=*electrosteric*) stabilization through the formation of an ion layer forming around the M-NPs. The type of this ion layer, hence, the mode of stabilization of metal nanoparticles in ILs is still a matter of some discussion [13,109]. Aside from the special case of thiol-, ether-, carboxylic acid-, amino-, hydroxyl- and other functionalized ILs (see Scheme 5 and accompanying text) one could decide between IL-cation or -anion coordination to the NP surface. Schrekker and co-workers proposed electrostatic stabilization of a negatively charged surface of Au-NPs by parallel coordination mode of the imidazolium cation on the basis of surface-enhanced Raman spectroscopy (SERS) studies [110]. This proposal was supported by Alvarez-Puebla and co-workers who found a negative zeta potential of M-NPs prepared by chemical reduction processes which indicated a negative charge of such NPs in aqueous solutions [111].

According to DLVO (Derjaugin–Landau–Verwey–Overbeek) theory (see Section 5) [112], ILs provide an electrostatic protection in the form of a "protective shell" for M-NPs [100,113–117]. DLVO theory predicts that the first inner shell must be anionic and the anion charges should be the primary source of stabilization for the electrophilic metal nanocluster [112]. DLVO theory treats anions as ideal point charges. Real-life anions with a molecular volume would be better classified as "*electrosteric* stabilizers" meaning to combine both the *electro*static and the *steric* stabilization. However, the term "electrosteric" is contentious and ill-defined [118]. The stabilization of metal nanoclusters in ILs could, thus, be attributed to "extra-DLVO" forces [118] which include effects from the network properties of ILs such as hydrogen bonding, the hydrophobicity and steric interactions [2,119].

Density functional theory (DFT) calculations in a gas phase model favor interactions between IL anions, such as BF_4^-, instead of imidazolium cations and Au_n clusters ($n = 1, 2, 3, 6, 19, 20$). This suggests a Au···F interaction and anionic Au_n stabilization in fluorous

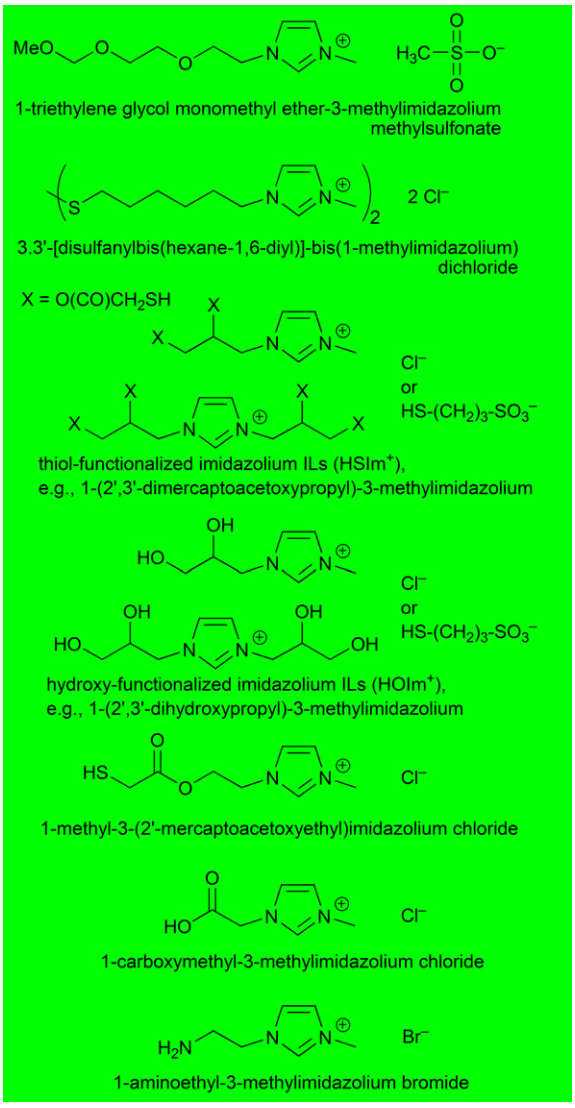

Scheme 5. Examples of functionalized imidazolium-ILs [108–110,124–126].

ILs. A small and Au-concentration dependent ^{19}F NMR chemical shift difference (not seen in ^{11}B- or ^1H NMR) for Au-NP/$BMIm^+BF_4^-$ supports the notion of a BF_4^--fluorine···Au-NP contact seen as crucial for the NP stabilization in dynamic ILs [120]. The DFT study used the binding energy (BE) of different IL-ions, free bases and the Cl^- anion to gold clusters of various sizes as a relative measure for the interaction strength.

The BE is defined as the difference of the relaxed energies of the gas phase anions and the Au_n clusters to the energy of their adduct (Eq. (1)) [120,121].

$$BE = E(\text{anion}) + E(Au_n) - E(\text{anion adduct to } Au_n) \quad (1)$$

Fig. 1 shows the Au_n–IL anion binding configurations and the variation of the BE with cluster size n. Fig. 2 illustrates Au_n–substrate binding configurations and the variation of the BE with cluster size n for BF_4^- in comparison with other common substrate ligands. The BE of $BMIm^+$ is very weak and not shown here (see in Refs. [120,121]). BE comparison with chloride, citrate, PH_3 and H_2O illustrates the critical influence of the ionic charge and electron delocalization from the ligand to Au_n (Fig. 2). The softer the anion or ligand, that is, the more charge transfer or electron delocalization (according to Pearsons hard-soft concept and the

Table 3
Examples of M-NPs prepared in ILs by chemical reduction.

Metal	Metal salt precursor	Reducing agent	IL[a]	M-NP size, average diameter (standard deviation) [nm]	Reference
Ru	Ru(COD)(COT)[b]	H_2	$BMIm^+Tf_2N^-$	0.9–2.4	[85]
	Ru(COD)(COT)[b]	H_2	$BMIm^+BF_4^-$, $BMIm^+PF_6^-$, $BMIm^+TfO^-$	2.6(4)	[104]
Rh	$RhCl_3{\cdot}3H_2O$	H_2	$BMIm^+PF_6^-$	2.0–2.5	[87]
	$[Rh(COD)\text{-}\mu\text{-}Cl]_2$[b]	H_2 + laser radiation	$BMIm^+PF_6^-$	7.2(1.3)	[127]
Ir	$[Ir(COD)Cl]_2$[b]	H_2	$BMIm^+BF_4^-$, $BMIm^+PF_6^-$, $BMIm^+TfO^-$	2–3	[128]
	$[Ir(COD)_2]BF_4$, $[Ir(COD)Cl]_2$[b]	H_2	1-alkyl-3-methyl-Im$^+BF_4^-$	Irregular 1.9(4), 3.6(9)	[89]
Pd	H_2PdCl_4	$NaBH_4$	$HSCO_2Im^+Cl^-$[c]	Nanowires	[125]
	$PdCl_2$	H_2 + laser radiation	$BMIm^+PF_6^-$	4.2(8)	[127]
	$Pd(acac)_2$	H_2	$BMIm^+PF_6^-$	10(2)	[91]
Pt	$Na_2Pt(OH)_6$	$NaBH_4$	$HSIm^+A^-$ or $HOIm^+A^-$[d]	3.2(1.1), 2.2(2), 2.0(1)	[124]
	H_2PtCl_6	$NaBH_4$	$CMMIm^+Cl^-$[e], $AEMIm^+Br^-$[f]	2.5	[109]
	PtO_2	H_2	$BMIm^+BF_4^-$, $BMIm^+PF_6^-$	2–3	[129]
Ag	$AgBF_4$	H_2	$BMIm^+BF_4^-$	2.8	[85]
			$BMIm^+PF_6^-$	4.4	[85]
			$BMIm^+TfO^-$	8.7	[85]
			$BtMA^+Tf_2N^-$	26.1	[85]
Au	$KAuCl_4$	$SnCl_2$	$BMIm^+BF_4^-$	2.6–200	[121]
	$HAuCl_4$	Na_3citrate/$NaBH_4$	$EMIm^+EtSO_4^-$	9.4	[131]
		Na_3citrate	$EMIm^+EtSO_4^-$	3.9	[131]
		Ascorbic acid	$EMIm^+EtSO_4^-$	Nanorods	[131]
	$HAuCl_4{\cdot}3H_2O$	$H_2NNH_2{\cdot}H_2O$ (hydrazine monohydrate)	$TriMIm^+MeSO_3^-$[g]	~7.5	[110]
	$HAuCl_4$	$NaBH_4$	$ShexMIm^+Cl^-$[h]	5.0	[108]
	$HAuCl_4$	$NaBH_4$	$HSIm^+A^-$ or $HOIm^+A^-$[d]	3.5(7), 3.1(5), 2.0(1)	[124]
	$HAuCl_4$	$NaBH_4$	$CMMIm^+Cl^-$[e], $AEMIm^+Br^-$[f]	3.5	[109]
	$HAuCl_4$	Na_3citrate	$CMMIm^+Cl^-$[e], $AEMIm^+Br^-$[f]	23–98	[109]
	$HAuCl_4$	Cellulose	$BMIm^+Cl^-$	300–800	[88]

[a] Common ILs: $BMIm^+BF_4^-$, $BMIm^+PF_6^-$, $BMIm^+TfO^-$ = 1-*n*-butyl-3-methylimidazolium tetrafluoroborate, hexafluorophosphate, trifluoromethylsulfonate, $BtMA^+Tf_2N^-$ *n*-butyl-trimethylammonium bis(trifluoromethylsulfonyl)amide (cf. Scheme 2); $EMIm^+EtSO_4^-$ = 1-ethyl-3-methylimidazolium ethylsulfate.
[b] COD = 1,5-cyclooctadiene, COT = 1,3,5-cyclooctatriene.
[c] $HSCO_2Im^+Cl^-$ = 1-methyl-3-(2′-mercaptoacetoxyethyl)imidazolium chloride (cf. Scheme 5).
[d] $HSIm^+A^-$ = thiol-functionalized imidazolium ILs, e.g., 1-(2′,3′-dimercaptoacetoxypropyl)-3-methylimidazolium, $HOIm^+A^-$ = hydroxy-functionalized imidazolium ILs, e.g., 1-(2′,3′-dihydroxypropyl)-3-methylimidazolium, A^- = Cl^- or HS-$(CH_2)_3$-SO_3^- (cf. Scheme 5).
[e] $CMMIm^+Cl^-$ = 1-carboxymethyl-3-methylimidazolium chloride (cf. Scheme 5).
[f] $AEMIm^+Br^-$ = 1-aminoethyl-3-methylimidazolium bromide (cf. Scheme 5).
[g] $TriMIm^+MeSO_3^-$ = 1-triethylene glycol monomethyl ether-3-methylimidazolium methylsulfonate (cf. Scheme 5).
[h] $ShexMIm^+Cl^-$ = 3.3′-[disulfanylbis(hexane-1,6-diyl)]-bis(1-methylimidazolium) dichloride.

nephelauxetic series) [122] to Au_n is possible, the better the stabilizing effect. H_2O as a hard and neutral ligand offers the least stabilization, hence, reduction of gold salts by $SnCl_2$ in water led immediately to the red purple solution (known as the Purple of Cassius). Remarkably, the relatively soft chloride anion shows the largest BE in agreement with the strong covalent binding of chloride ions to the Au(1 1 1) surface found in recent DFT simulations [123].

The DFT calculations also indicate a weak covalent part in this Au···F interaction. Free imidazole bases (e.g., 1-methylimidazole) show similar binding energies. The Cl^- anions have the highest binding energy and can therefore be expected to bind to the NP if present in the solution. At the same time no significant binding of the $BMIm^+$ or MIm^+ imidazolium cations is found. These findings support the model of preferred interaction between anions and Au-NPs, but also confirm the importance to consider a possible presence of Cl^- anions in the ionic liquid solution [120,121].

Compared with the non-functionalized imidazolium-ILs (cf. Scheme 2), functionalized imidazolium-ILs stabilize aqueous dispersed metal NPs much more efficiently because of the special functional group. Thiol-functionalized [108,124,125], ether-functionalized [110], carboxylic acid-functionalized [109], amino-functionalized [109,126], and hydroxyl-functionalized [124] imidazolium-ILs (Scheme 5) have been used to synthesize aqueous dispersed noble, primarily gold metal NPs.

4.1. Chemical reduction

The reduction of metal salts is the most utilized method to generate NPs in solution and also in ILs in general. Many different types of reducing agents are used, like gases (H_2), organic (citrate, ascorbic acid, imidazolium cation of IL) and inorganic ($NaBH_4$, $SnCl_2$) agents (Table 3).

Molecular hydrogen (H_2) is often taken as clean reductant. Dupont et al. used $RhCl_3{\cdot}3H_2O$ as a precursor in $BMIm^+PF_6^-$ for the formation of Rh-NPs. For Ir-NPs the precursor $[Ir(COD)Cl]_2$ (COD = 1,5-cyclooctadiene) was reduced with H_2. The formation to M-NPs was carried out at 75 °C and 4 bar hydrogen pressure. Transmission electron microscopy (TEM) analysis showed the particle sizes of 2.0–2.5 nm [87]. Redel et al. used hydrogen and $AgBF_4$ for the synthesis of Ag-NPs in different ILs. A correlation between the IL-anion molecular volume and the NP size was noted. The larger the volume of the IL-anion the larger is the size of the Ag-NPs. Thereby it was possible to form Ag-NPs in sizes from 2.8 to 26.1 nm with a narrow size distribution [84].

Different researchers used hydrogen as a reagent not to reduce the metal but to reduce (hydrogenate) the ligands COD and COT (COT = 1,3,5-cyclooctatriene) of an Ru(0) organometallic precursor [85,104]. They dissolved Ru(COD)(COT) in imidazolium based ILs and heated the mixture under 4 bar of hydrogen under different conditions. Both organic ligands were reduced to cyclooctane and thereby dissociate from the already zero-valent metal atom. Cyclooctane can then be removed under reduced pressure.

It is also possible to use less-noble metals for the reduction of noble metals. The reduction of $KAuCl_4$ by $SnCl_2$ leads to the formation of Au-NPs [121]. By variation of the molar Au(III):Sn(II) ratio it was possible to synthesize Au-NPs in different sizes in a stop-and-go, stepwise and "ligand-free" nucleation, nanocrystal growth process which can be stopped and resumed at different color steps

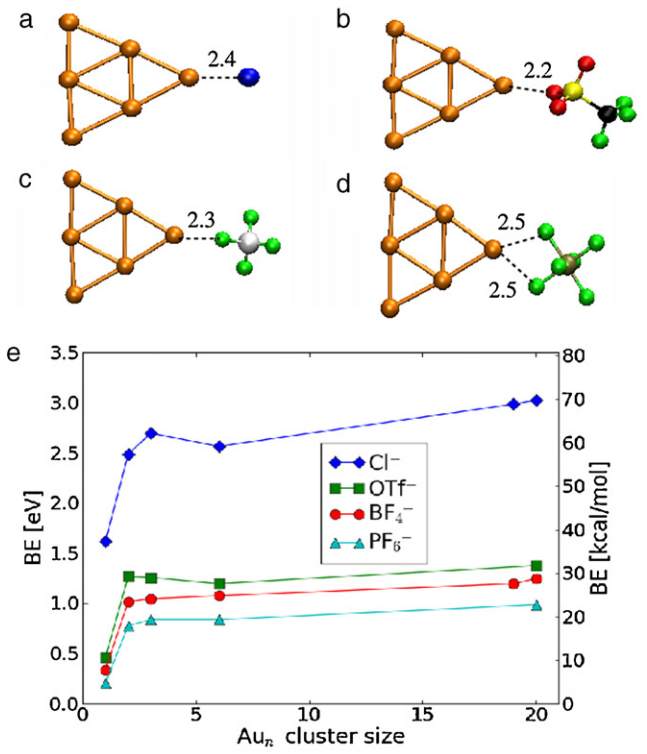

Fig. 1. Relaxed configurations of Au_6 bound to (a) Cl^-, (b) TfO^-, (c) BF_4^- and (d) PF_6^-. The bond lengths are given in Å. (e) Binding energy. All the anions show a similar behavior in their BE: the BE to a single gold atom $n = 1$ is quite low and more than doubles for Au_2 ($n = 2$). Increasing the cluster size to $n = 20$ does not change the BE substantially anymore, i.e., the BE is already saturated for Au_2. The chloride anion shows the largest BE of all anions and can, hence, be expected to be bound to the clusters if it is present in the dispersion [120].

and Au-NP sizes from 2.6 to 200 nm. This stepwise Au-NP formation was possible because the IL apparently acted as a *kinetically* stabilizing, dynamic molecular network in which the reduced Au^0 atoms and clusters can move by diffusion and cluster together, as verified by TEM analysis [121].

A well-known method to generate Au-NPs was already established by Turkevich et al. in 1951 [130]. The reducing agent was citrate. Bockstaller and coworkers used this method and carried out the reduction in the imidazolium-based IL 1-ethyl-3-methylimidazolium ethyl-sulfate ($EMIm^+EtSO_4^-$). Afterwards it was possible to give these particles different shapes by adding Ag(I) [131].

Taubert et al. reacted $HAuCl_4$ with cellulose [88]. Thereby cellulose has two roles: first, cellulose is the reducing agent for Au(III). Second, cellulose acts as a morphology- and size-directing agent, which drives the crystallization towards polyhedral particles or thick plates. The gold particle morphologies and sizes mainly depend on the reaction temperature. With this route it was possible to synthesize plates with a thickness from 300 nm at 110 °C to 800 nm at 200 °C.

Gold nanoparticles of 1–4 nm size could be prepared by sputter deposition of the metal onto the surface of the ionic liquid $BMIm^+BF_4^-$ to generate nanoparticles in the liquid with no additional stabilizing agents [132]. Likewise, Au-NPs were prepared by sputter deposition of Au metal in $BMIm^+PF_6^-$. The size of Au nanoparticles was increased from 2.6 to 4.8 nm by heat treatment at 373 K [133]. Sputter deposition of indium in the ionic liquids $BMIm^+BF_4^-$, $EMIm^+BF_4^-$, (1-allyl)$MIm^+BF_4^-$ and (1-allyl)(3-ethyl)$Im^+BF_4^-$ could produce stable In metal nanoparticles whose surface was covered by an amorphous In_2O_3 layer to form In/In_2O_3 core/shell particles. The size of the In core was tunable from ca. 8 to 20 nm by selecting the IL [134].

Mudring and coworkers evaporated elemental Cu powder under high vacuum (10^{-6} torr) into the IL 1-butyl-3-methylimidazolium hexafluorophosphate and generated Cu nanoparticles with the size of 3 nm. Au nanoparticles were prepared with the same evaporation method. Depending on the different ILs which were used, nanoparticles from 4 to 50 nm were generated. This method made it also possible to produce Cu/ZnO nanocomposites [135].

Dupont et al. prepared Au-NPs with the size of 3–5 nm from gold foil by sputtering deposition onto several imidazolium-based ILs. [136].

In the presence of imidazolium-based ILs Pd-NPs from palladium(II) salts could be synthesized without the need for an additional reducing agent. It is suggested that formation of *N*-heterocyclic Pd-carbene complexes takes place as an intermediate preceding the formation of Pd-NPs (Scheme 6) which can then catalyze Suzuki C–C coupling reactions [92,137]. Pd-carbene complexes are able to catalyze the Heck reaction [138,139].

Deshmukh et al. used $Pd(OAc)_2$ or $PdCl_2$ in the imidazolium-based ILs BBImBr or $BBImBF_4$ to irradiate the mixtures with

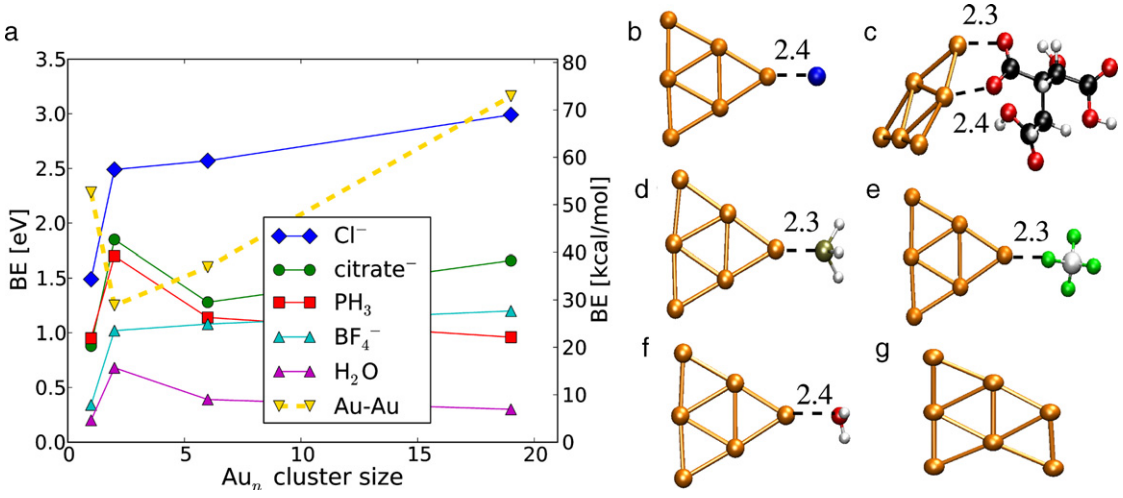

Fig. 2. (a) Binding energies (BE) and Au-atom addition energies depending on the cluster size. (b–f) Relaxed configurations of Au_6 bound to (b) Cl^-, (c) citrate$^-$ ($C_6H_7O_7^-$), (d) PH_3, (e) BF_4^- and (f) H_2O. (g) Relaxed configuration of Au_7. The bond lengths are given in Å [121].

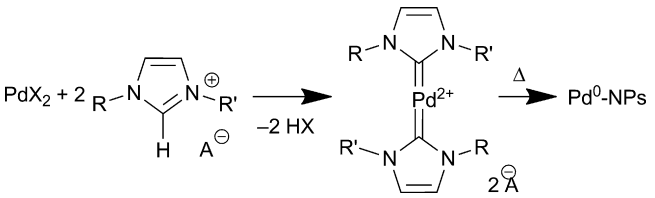

Scheme 6. Reduction of Pd(II)-species with an imidazolium-based IL through intermediate formation of Pd-carbene complexes. Decomplexation and reduction occurs during heating.

ultrasound for 1 h. The Pd-NPs were nearly spherical and a size of 20 nm was observed [92].

Anderson, Marr et al. formed Pd-NPs with a diameter of ~1 nm from $Pd(OAc)_2$ in $BMIm^+Tf_2N^-$ simply by heating to 80 °C in the presence of PPh_3 [93].

Ruta et al. synthesized monodisperse Pd nanoparticles of 5 and 10 nm through reduction of $Pd(acac)_2$ dissolved in the hydroxyl-functionalized butyl-3-methylimidazolium bis(trifluoromethylsulfonyl)amide IL $HOBMIm^+Tf_2N^-$ by simple heating in the absence of an additional reducing agent [91].

D/H exchange reactions at C2, C4 and C5 of the imidazolium cation in catalytic hydrogenation reactions promoted by classical Ir(I) colloid precursors and Ir-NPs in deuterated imidazolium ILs supported the participation of carbene species in this media [140].

Also by thermal decomposition, albeit from an Ni(0) source, Ni nanoparticles with 4.9(9) to 5.9(1.4) nm average diameter (standard deviation) were prepared from the bis(1,5-cyclooctadiene)nickel(0) organometallic precursor dissolved in 1-alkyl-3-methylimidazolium bis(trifluoromethylsulfonyl)amide ionic liquids [90].

Carboxylic acid- and amino-functionalized ionic liquids $CMMIm^+Cl^-$ = 1-carboxylmethyl-3-methylimidazolium chloride and $AEMIm^+Br^-$ = 1-aminoethyl-3-methylimidazolium bromide (cf. Scheme 5) were used as the stabilizer for the synthesis of gold and platinum metal nanoparticles in aqueous solution. Smaller Au-NPs (3.5 nm) and Pt-NPs (2.5 nm) were prepared with $NaBH_4$ as the reductant. Larger gold nanospheres (23, 42, and 98 nm) were synthesized using different quantities of trisodium citrate reductant. The morphology and the surface state of the metal nanoparticles were characterized by high-resolution transmission electron microscopy, UV–vis spectroscopy, and X-ray photoelectron. X-ray photoelectron spectra indicated that binding energies of C 1s and N 1s from ionic liquids on the surface of metal nanoparticles shifted negatively compared with that from pure ionic liquids. The mechanism of stabilization is proposed to be due to the interactions between imidazolium ions/functional groups in ionic liquids and metal atoms. The imidazolium ring moiety of ionic liquids might interact with the π-electronic nanotube surface by virtue of cation–π and/or π–π interactions, and the functionalized group moiety of ionic liquids might interact with the metal NPs surface [109].

4.2. Photochemical reduction

Photochemical methods for the synthesis of M-NPs present a rather clean procedure because contaminations by reducing agents are excluded.

Zhu et al. used $HAuCl_4{\cdot}4H_2O$ in a mixed solution of $BMIm^+BF_4^-$ and acetone (ratio 10:1) and irradiated the salt for 8 h with a UV light at a wavelength of 254 nm. The UV light turns the acetone into a free radical, which then reduces the cationic Au(III) to Au-NPs. The obtained Au nanosheets were about 4 μm long and 60 nm thick [94].

Firestone et al. used this route to form Au-NPs from $HAuCl_4$ in the IL 1-decyl-3-methyl-imidazolium chloride in water. The irradiation was carried out with 254 nm UV light for 30–70 min. The obtained Au-NPs were analyzed by scanning electron microscopy (SEM). The nanorods had different shapes and morphologies. The sizes varied between 100 and 1000 nm [95].

Harada et al. used a high-pressure mercury lamp to irradiate $AgClO_4$ in a mixture of an IL, water and Tween 20 (polyoxyethylene sorbitan monolaurate). Benzoin was used as photoactivator. The average diameters of Ag-NPs prepared in water/$BMIm^+BF_4^-$ and water/$OMIm^+BF_4^-$ (1-octyl-3-methylimidazolium) microemulsions were 8.9 and 4.9 nm, respectively [141].

4.3. Electroreduction

Another clean route to prepare nanoparticles is electroreduction as only electrons are used as the reducing agent. It should be noted, however, that the size of the metal nanoparticles from electroreduction is often above the 100 nm definition limit for nanoparticles.

Imanishi et al. used a low-energy electron beam irradiation to synthesize Au-NPs from a $NaAuCl_4{\cdot}2H_2O$ precursor in the IL $BMIm^+Tf_2N^-$. The obtained particles had a large size of 122 nm [142].

It is also possible to deposit particles on supporting material. Roy et al. prepared Ag-NPs from $AgBF_4$ in $BMIm^+BF_4^-$ on TiO_2. The electroreduction was performed in the high vacuum chamber of a SEM. The resulting Ag-NPs arranged themselves in a dendritic network structure [143].

Fu et al. reduced graphene oxide (GO) and $HAuCl_4$ simultaneously in $BMIm^+PF_4^-$ at a potential of −2.0 V. The obtained Au-NPs on the electrochemical reduced graphene had a size of 10 nm [144].

El Abedin and Endres used Ag(TfO) as a source of silver. The precursor was electrochemically reduced in 1-ethyl-3-methylimidazolium trifluoromethylsulfonate, $EMIm^+TfO^-$. The prepared Ag nanowires were 3 μm long and 200 nm wide [145].

CuCl as precursor was used by Lu et al. and reduced in a cavity microelectrode in $BMIm^+PF_6^-$. The electrode potential was varied. The smallest particles had a size of 10 nm and were obtained at an electrode potential of −1.8 V [146].

4.4. Metal carbonyl precursors for metal nanoparticles in ILs

As pointed out in Section 3 metal carbonyls contain the metal atoms already in the zero-valent oxidation state needed for the metal nanoparticles. No reducing agent is necessary. The side product CO is largely given off to the gas phase and removed from the M-NP/IL dispersion. The M-NP synthesis in IL from $M_x(CO)_y$ is generally carried out without any additional stabilizers, surfactants or capping molecules which is different from the use of metal carbonyls for the M-NP syntheses described in Section 3. Metal carbonyls can be decomposed to metal nanoparticles in ILs by conventional thermal heating, UV-photolysis or microwave irradiation (MWI) (Fig. 3a–c).

ILs are an especially attractive media for microwave reactions and have significant absorption efficiency for microwave energy because of their high ionic charge, high polarity and high dielectric constant [18]. Microwave heating is extremely rapid. Microwaves are a low-frequency energy source that is remarkably adaptable to many types of chemical reactions [147]. Microwave radiation can interact directly with the reaction components: the reactant mixture absorbs the microwave energy and localized superheating occurs resulting in a fast and efficient heating time [148,149]. Using microwaves is a fast way to heat reactants compared with conventional thermal heating. Any presumptions about abnormal "microwave effects" [150–152] have been proven wrong in the

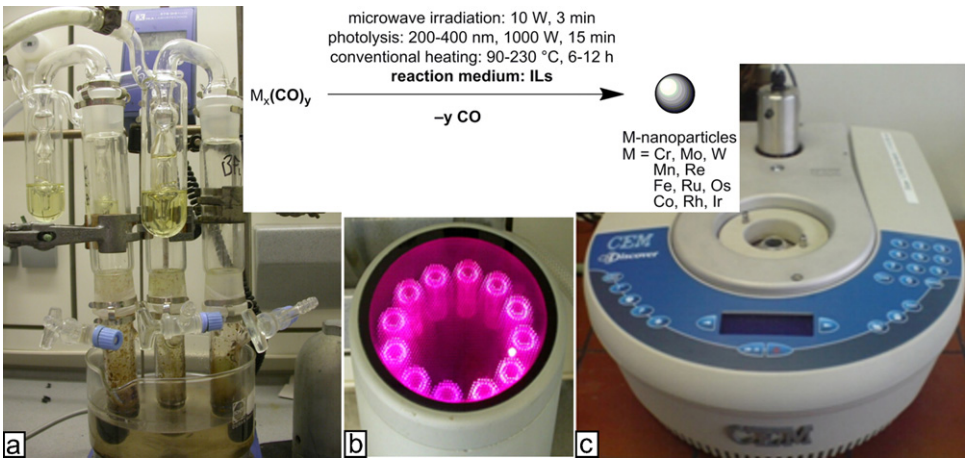

Fig. 3. (a) Setup for conventional thermal heating of $M_x(CO)_y$/IL dispersions under argon, (b) UV reactor, (c) commercial laboratory microwave reactor.

meantime [153,154]. Moreover, microwave reactions are also an "instant on/instant off" energy source, significantly reducing the risk of overheating reactions [147,148].

Metal nanoparticles (M-NPs) were reproducibly obtained by easy, rapid (3 min) and energy-saving 10 Watt microwave irradiation (MWI) under an argon atmosphere from their metal carbonyl precursors $M_x(CO)_y$ in ILs. This MWI synthesis was compared to UV-photolytic (1000 W, 15 min) or conventional thermal decomposition (180–250 °C, 6–12 h) of $M_x(CO)_y$ in ILs. The MWI-obtained nanoparticles have a very small (<5 nm) and uniform size and are prepared without any additional stabilizers or capping molecules as long-term stable M-NP/IL dispersions [characterization by transmission electron microscopy (TEM), transmission electron diffraction (TED) and dynamic light scattering (DLS)].

Stable chromium, molybdenum and tungsten nanoparticles could be obtained reproducibly by thermal or photolytic decomposition under argon from their mononuclear metal carbonyl precursors $M(CO)_6$ (M = Cr, Mo, W) suspended in the ionic liquids $BMIm^+BF_4^-$, $BMIm^+TfO^-$ and $BtMA^+Tf_2N^-$ (Scheme 7) [99]. Later an even more rapid and energy-saving decomposition could be achieved with a 10 W microwave irradiation for 3 min of 0.4 ml (0.48 g) of a $BMIm^+BF_4^-$ sample with a 0.5 wt.% M/IL-dispersion [21]. The resulting Cr-, Mo- and W-NPs were of very small and uniform size of 1–1.5 nm in $BMIm^+BF_4^-$ (Table 4) which increases with the molecular volume of the ionic liquid anion to ~30–100 nm in $BtMA^+Tf_2N^-$ (Fig. 4). Characterization was done by TEM, dynamic light scattering (DLS) and transmission electron diffraction (TED) analysis [99].

Complete $M(CO)_6$ decomposition from the short, 3 min microwave irradiation was verified by Raman spectroscopy with no (metal-)carbonyl bands between 1750 and 2000 cm^{-1} being observed any more after the microwave treatment (Fig. 5) [21].

Stable manganese and rhenium metal nanoparticles were reproducibly obtained by microwave irradiation or UV photolysis from their metal carbonyl precursors $M_2(CO)_{10}$ in the ionic liquid 1-butyl-3-methylimidazolium tetrafluoroborate ($BMIm^+BF_4^-$) (Scheme 8, Fig. 6, Table 4) [21].

Complete $M_2(CO)_{10}$ decomposition from the short, 3 min microwave irradiation was verified by Raman spectroscopy with no (metal-)carbonyl bands between 1750 and 2000 cm^{-1} being observed any more after the microwave treatment (Fig. 7) [21].

Stable iron, ruthenium and osmium nanoparticles are obtained reproducibly by microwave irradiation, photolytic or conventional thermal decomposition under argon atmosphere from $Fe_2(CO)_9$, $Ru_3(CO)_{12}$ or $Os_3(CO)_{12}$, dissolved in the ionic liquid $BMIm^+BF_4^-$ and with a very small and uniform size for Ru and Os nanoparticles of about 1.5–2.5 nm without any additional stabilizers or capping molecules (Scheme 9, Figs. 8–10, Table 4) [9,21].

Complete $M_x(CO)_y$ (M = Fe, Ru, Os) decomposition from the short, 3 min microwave irradiation was verified by Raman spectroscopy with no (metal-)carbonyl bands between 1750 and 2000 cm^{-1} being observed any more after the microwave treatment (Fig. 10) [21].

The Ru-NP/$BMIm^+BF_4^-$ and other M-NP/IL dispersions were active catalysts in the biphasic liquid–liquid hydrogenation of cyclohexene or benzene to cyclohexane. Even a remarkable partial hydrogenation of benzene to cyclohexene could be achieved with

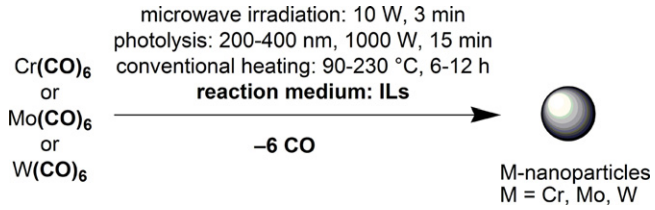

Scheme 7. Formation of Cr, Mo and W nanoparticles by microwave, photolytic or thermal decomposition of metal carbonyls $M(CO)_6$ under argon in ionic liquids [21,99].

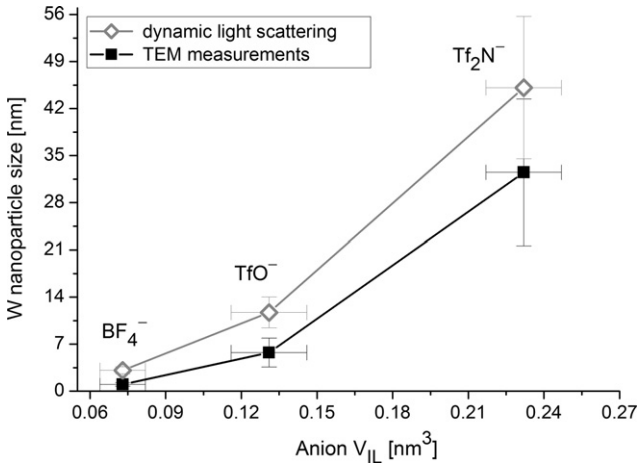

Fig. 4. Correlation between the molecular volume of the ionic liquid anion (V_{IL}) and the observed W nanoparticle size with standard deviations as error bars (from TEM and dynamic light scattering). IL anions range from BF_4^- (smallest) over trifluoromethylsulfonate (triflate, $CF_3SO_3^-$, TfO^-) to the largest bis(trifluoromethylsulfonyl)amide [$(CF_3SO_2)_2N^-$, Tf_2N^-] [99].

Table 4
M-NP (M = Cr, Mo, W, Re, Mn, Fe, Ru, Os, Co, Rh and Ir) size and size distribution in $BMIm^+BF_4^-$ [21].[a]

Entry	Metal carbonyl	Microwave decomposition[b]		Photolytic decomposition[c]		Conventional thermal decomposition[d]	
		TEM NP diameter/nm (standard deviation σ)	Dynamic light scattering NP median diameter[e]/nm (standard deviation σ)	TEM NP diameter/nm (standard deviation σ)	Dynamic light scattering NP median diameter[e]/nm (standard deviation σ)	TEM NP diameter/nm (standard deviation σ)	Dynamic light scattering NP median diameter[e]/nm (standard deviation σ)
1	$Cr(CO)_6$	≤1.5 (±0.3)[f]	3.8 (±0.8)	4.4 (±1.0)	7.1 (±0.3)	≤1.5 (±0.3)[g]	3.0 (±0.6)[g]
2	$Mo(CO)_6$	~1–2	4.5 (±0.8)	~1–2[g]	3.8 (±1.1)[g]	≤1.5 (±0.3)[g]	2.5 (±0.6)[g]
3	$W(CO)_6$	3.1 (±0.8)	5.2 (±1.2)	<1	10.8 (±0.5)	≤1.5 (±0.3)[g]	3.1 (±0.5)[g]
4	$Mn_2(CO)_{10}$	12.4 (±3)[h]	29 (±5.0)[h]	<1	2.5 (±0.8)	–	–
5	$Re_2(CO)_{10}$	2.4 (±0.9)	5.7 (±1.4)	<1	7.2 (±2.2)	–	–
6	$Fe_2(CO)_9$	8.6 (±3.2)[i]	12.8 (±0.6)[i]	7.0 (±3.1)[i]	12.5 (±0.5)[i]	5.2 (±1.6)[g]	10.1 (±2.1)[g]
7	$Ru_3(CO)_{12}$	(a) 1.6 (±0.3) (b) 1.6 (±0.3)[j]	(a) 3.2 (±0.8) (b) 3.2 (±0.8)[j]	2.0 (±0.5)[g]	3.9 (±1.0)[g]	1.6 (±0.4)[g]	2.9 (±0.5)[g]
8	$Os_3(CO)_{12}$	0.7 (±0.2)	2.8 (±0.7)	2.0 (±1.0)	2.1 (±0.4)	2.5 (±0.4)[g,k]	5.6 (±1.5)[l]
9	$Co_2(CO)_8$	5.1 (±0.9)	20 (±3)	8.1 (±2.5)	12.6 (±0.4)	14 (±8)[g]	–
10	$Rh_6(CO)_{16}$	(a) 1.7 (±0.3) (b) 1.7 (±0.3)[j]	3.7 (±0.6) 3.4 (±0.5)[j]	1.9 (±0.3)	5.5 (±0.4)	3.5 (±0.8)[g]	7.0 (±1.2)[g]
11	$Ir_6(CO)_{16}$	0.8 (±0.2)	3.3 (±0.9)	1.4 (±0.3)	4.1 (±1.2)	(a) 1.1 (±0.2)[g] (b) 1.3 (±0.2)[g,m]	4.1 (±0.7)[g]3.4 (±1.0)[g,m]

[a] Median diameters and standard deviations are for a single TEM or DLS experiment. Reproducibility of the particle size and distribution was insured by selected repeated TEM experiments and especially by DLS which was carried out for almost all repeated decomposition reactions. Solubility of metal carbonyl precursors in $BMIm^+BF_4^-$ is limited to a maximum value of about 1 wt.% M.

[b] Microwave decomposition of metal carbonyls with 10 W for 3 min unless mentioned otherwise.

[c] Photolytic decomposition of metal carbonyls with a 1000 W Hg lamp (200–450 nm wavelength) for 15 min.

[d] Thermal decomposition of metal carbonyls from 6 to 12 h with 180–230 °C depending on the metal carbonyl.

[e] Hydrodynamic radius, median diameter from the first three measurements at 633 nm. Only the first three scans are somewhat reliable, because the laser light used for the measurements induces clustering of the nanoparticles upon repeated number of scans. The hydrodynamic radius is roughly 2–3 times the size of the pure kernel cluster. For very small M-NPs (~1 nm) the size of the hydrodynamic radius can even increase to more than 3 times the M-NP radius. The resolution of the DLS instrument is 0.6 nm.

[f] TEM pictures with particles of median diameter of less than 1.5 nm show electron dense cloudy structures due to scattering by the surrounding IL so that resolution of the TEM is limited and particles below 1.5 nm are hardly resolved.

[g] Data from Refs. [9,20,99].

[h] $Mn_2(CO)_{10}$ was of larger grain size than all the other metal carbonyls which came as fine powders. Also upon grinding in a mortar, $Mn_2(CO)_{10}$ could not be as finely powdered as the other metal carbonyls.

[i] TEM/TED analyses of the nanoparticles from the microwave and photolytic decomposition of $Fe_2(CO)_9$ show the presence of iron oxide, Fe_2O_3. Because of the experimental setup rigorous air exclusion is more difficult during the microwave irradiation and photolysis and workup.

[j] Microwave decomposition of metal carbonyls with 10 W for 10 min.

[k] 0.2 wt.% $Os_3(CO)_{12}$ in $BMIm^+BF_4^-$.

[l] 1 wt.% $Os_3(CO)_{12}$ in $BMIm^+BF_4^-$.

[m] 18 h decomposition time of 0.5 wt.% $Ir_4(CO)_{12}$ in $BMIm^+BF_4^-$.

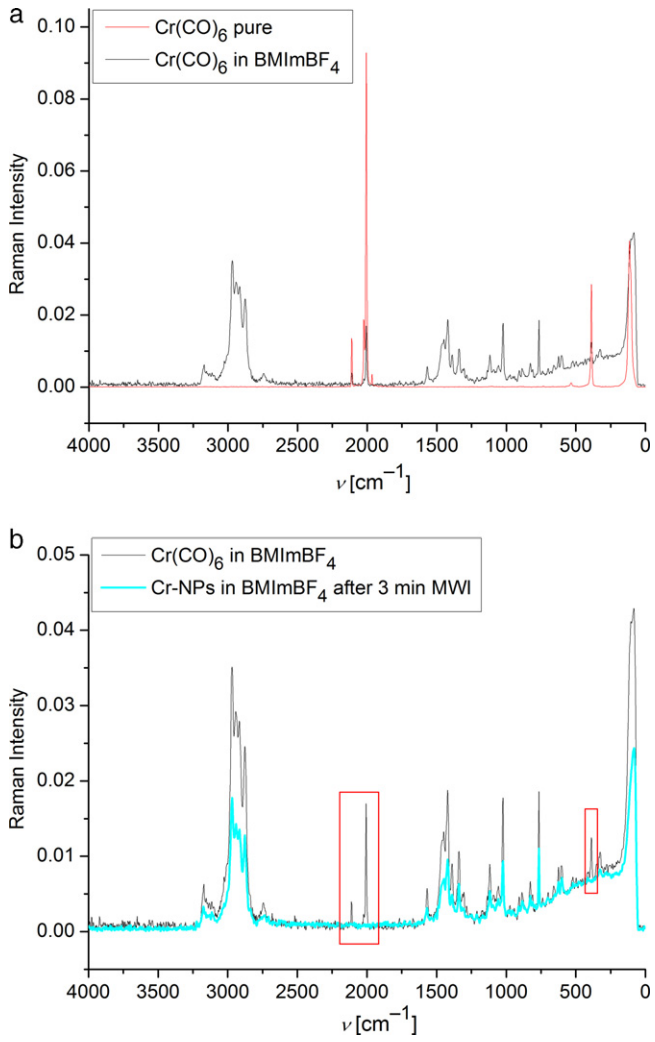

Fig. 5. Raman-FT spectra. Top: pure $Cr(CO)_6$ and $Cr(CO)_6$ in $BMIm^+BF_4^-$; bottom: $Cr(CO)_6$ in $BMIm^+BF_4^-$ before and after 3 min 10 W microwave irradiation (MWI). Red boxes highlight the indicative chromium carbonyl bands [21].

Ru-NP/$BMIm^+PF_6^-$ dispersions [105]. The low miscibility of substrates and products with the IL phase allows for easy separation by simple decantation of the hydrophobic phase [19]. The hydrogenation reaction of cyclohexene was run at 90 °C and 10 bar H_2 to 95% conversion where the reaction was intentionally stopped as thereafter the decrease in cyclohexene concentration lowered the reaction rate (Fig. 11) [21].

Silva, Dupont et al. have prepared cobalt nanoparticles with a size of around 7.7 nm by the decomposition of $Co_2(CO)_8$ in 1-alkyl-3-methylimidazolium Tf_2N^- ionic liquids at 150 °C. These Co-NPs were effective catalysts for the Fischer–Tropsch (FT) synthesis,

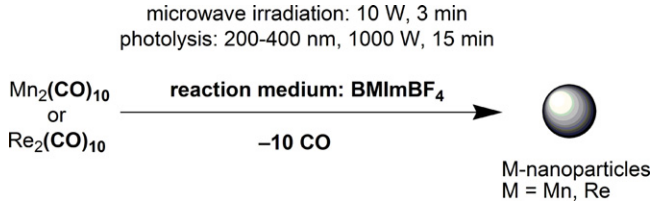

Scheme 8. Formation of Mn and Re nanoparticles by microwave, photolytic or thermal decomposition of the metal carbonyls $M_2(CO)_{10}$ under argon in the IL $BMIm^+BF_4^-$ [21].

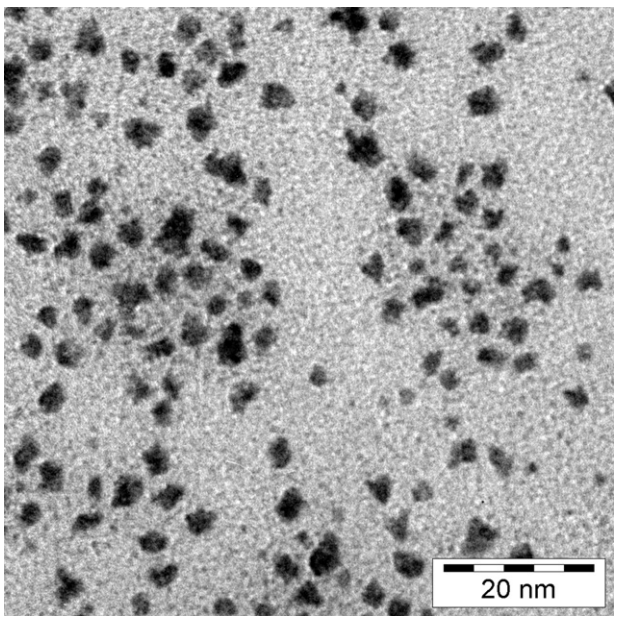

Fig. 6. TEM photograph of Re-NPs from $Re_2(CO)_{10}$ by MWI (Ø 2.4 (±0.9) nm, entry 5 in Table 4) [21].

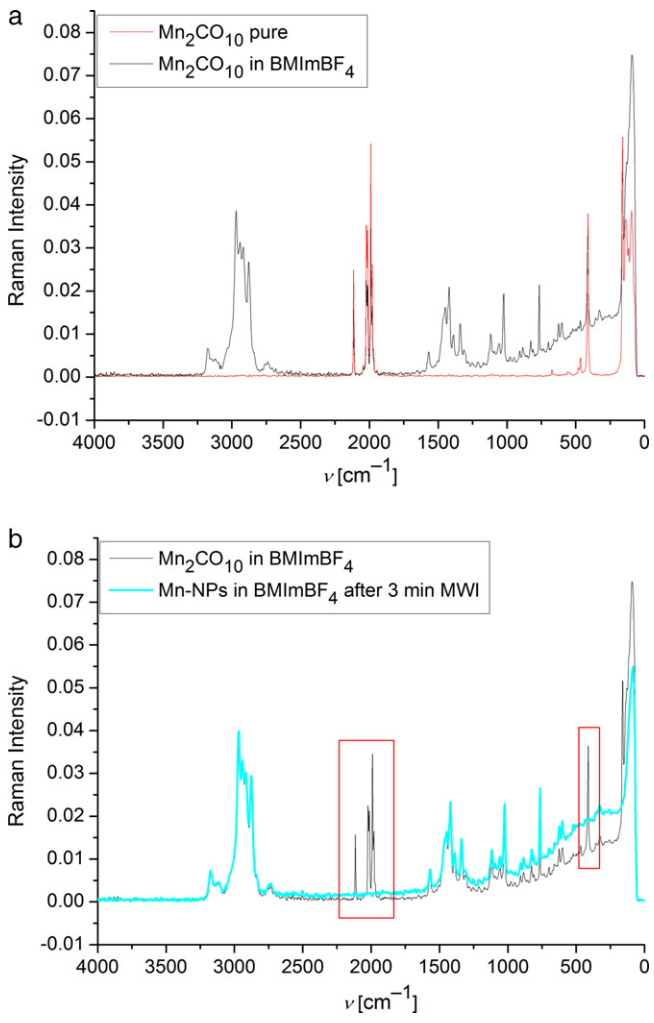

Fig. 7. Raman-FT spectra. Top: pure $Mn_2(CO)_{10}$ and $Mn_2(CO)_{10}$ in $BMIm^+BF_4^-$; bottom: $Mn_2(CO)_{10}$ in $BMIm^+BF_4^-$ before and after 3 min 10 W microwave irradiation (MWI). Red boxes highlight the indicative manganese carbonyl bands [21].

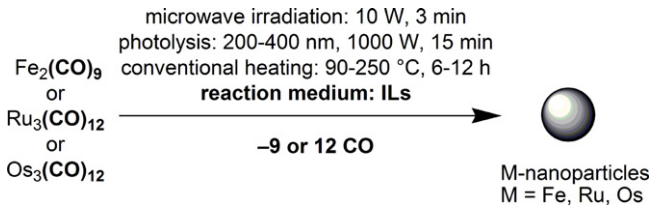

Scheme 9. Formation of Fe, Ru and Os nanoparticles by microwave, photolytic or thermal decomposition of metal carbonyls $M_x(CO)_y$ under argon in the IL $BMIm^+BF_4^-$ [9,21].

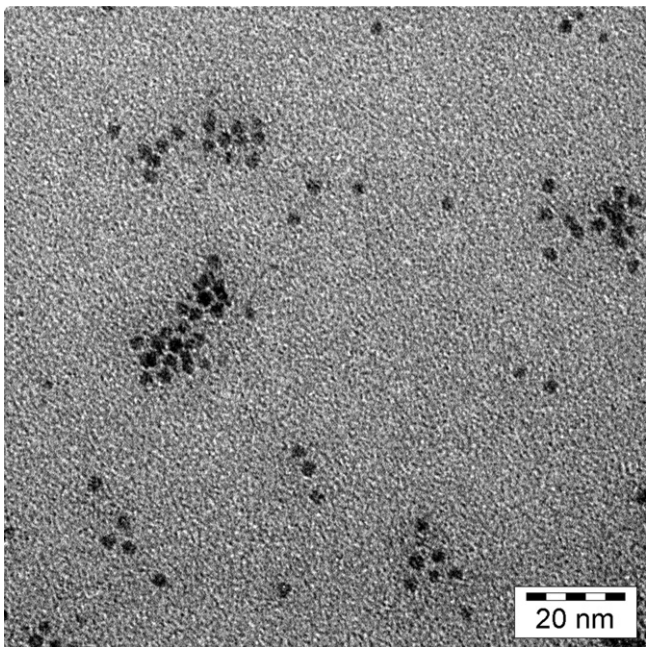

Fig. 8. TEM photograph of Ru-NPs from $Ru_3(CO)_{12}$ by photolytic decomposition (0.08 wt.% Ru in $BMIm^+BF_4$) (Ø 2.0 (±0.5) nm, entry 7 in Table 4) [9].

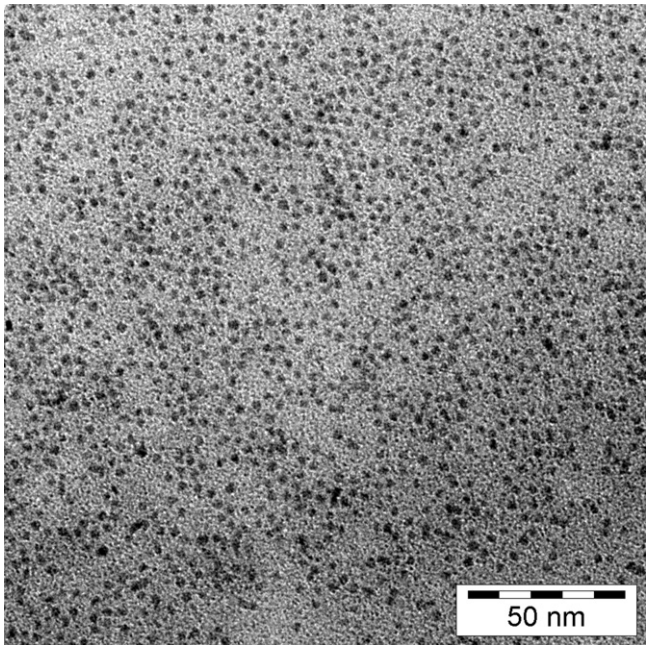

Fig. 9. TEM photograph of Os-NPs from $Os_3(CO)_{12}$ by conventional thermal decomposition (0.2 wt.% Os in $BMIm^+BF_4^-$) (Ø 2.5 (±0.4) nm, entry 8 in Table 4) [9].

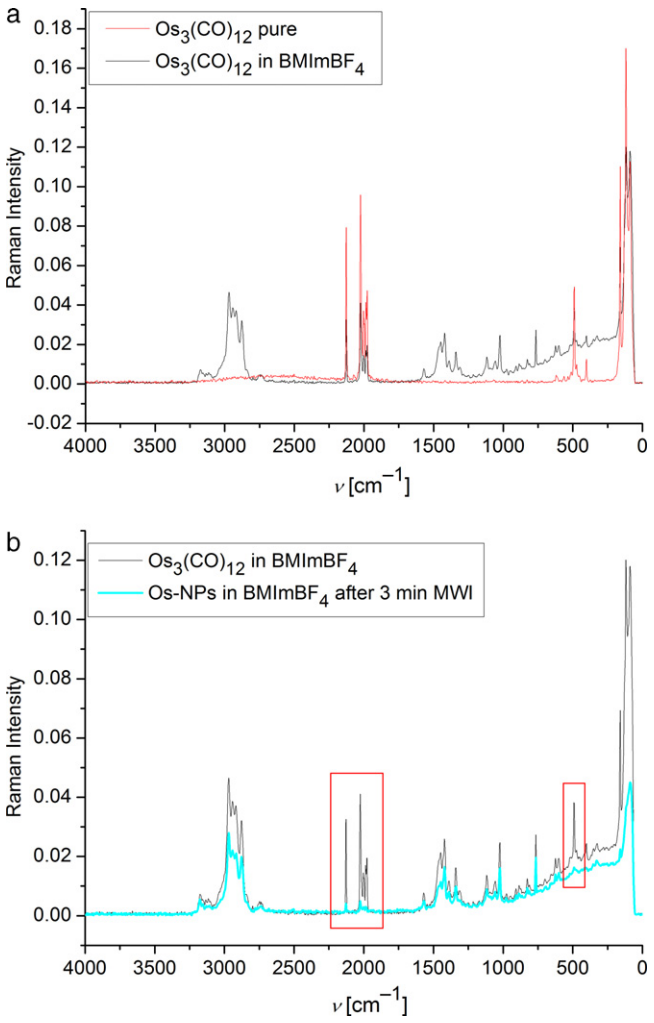

Fig. 10. Raman-FT spectra. Top: pure $Os_3(CO)_{12}$ and $Os_3(CO)_{12}$ in $BMIm^+BF_4^-$; bottom: $Os_3(CO)_{12}$ in $BMIm^+BF_4^-$ before and after 3 min 10 W microwave irradiation (MWI). Red boxes highlight the indicative osmium carbonyl bands [21].

yielding olefins, oxygenates, and paraffins (C_7–C_{30}) and could be reused at least three times if they were not exposed to air [155].

The decomposition of $Co_2(CO)_8$ dispersed in 1-*n*-decyl-3-methylimidazolium bis(trifluoromethylsulfonyl)amide ($DMIm^+Tf_2N^-$) at 150 °C over 1 h afforded a black solution containing Co-NPs with a cubic shape (53 ± 22 nm), together with Co-NPs of irregular shape [156].

Stable cobalt, rhodium and iridium nanoparticles were obtained reproducibly by thermal decomposition under argon from $Co_2(CO)_8$, $Rh_6(CO)_{16}$ and $Ir_4(CO)_{12}$ dissolved in the ionic liquids $BMIm^+BF_4^-$, $BMIm^+TfO^-$ and $BtMA^+Tf_2N^-$ (Scheme 10, Fig. 12, Table 4) [20]. Later an even more rapid and energy-saving decomposition could be achieved with a 10 W microwave irradiation for 3 min of 0.4 ml (0.48 g) of a $BMIm^+BF_4^-$ sample with a 0.5 wt.% $M_x(CO)_y$/IL-dispersion to yield the M-NP/IL-dispersion [21]. The very small and uniform nanoparticle size of about 1–3 nm for the Co-, Rh- or Ir-NPs in $BMIm^+BF_4^-$ (Table 4) increases with the molecular volume of the ionic liquid anion in $BMIm^+TfO^-$ and $BtMA^+Tf_2N^-$ (Fig. 13). Characterization of the nanoparticles was done by TEM, transmission electron diffraction (TED), X-ray powder diffraction (XRPD) and dynamic light scattering (DLS). The rhodium or iridium nanoparticle/IL systems function as highly effective and recyclable catalysts in the biphasic liquid-liquid hydrogenation of cyclohexene to cyclohexane with activities of up to 1900 mol cyclohexane × $(\text{mol Ir})^{-1}$ × h^{-1} and

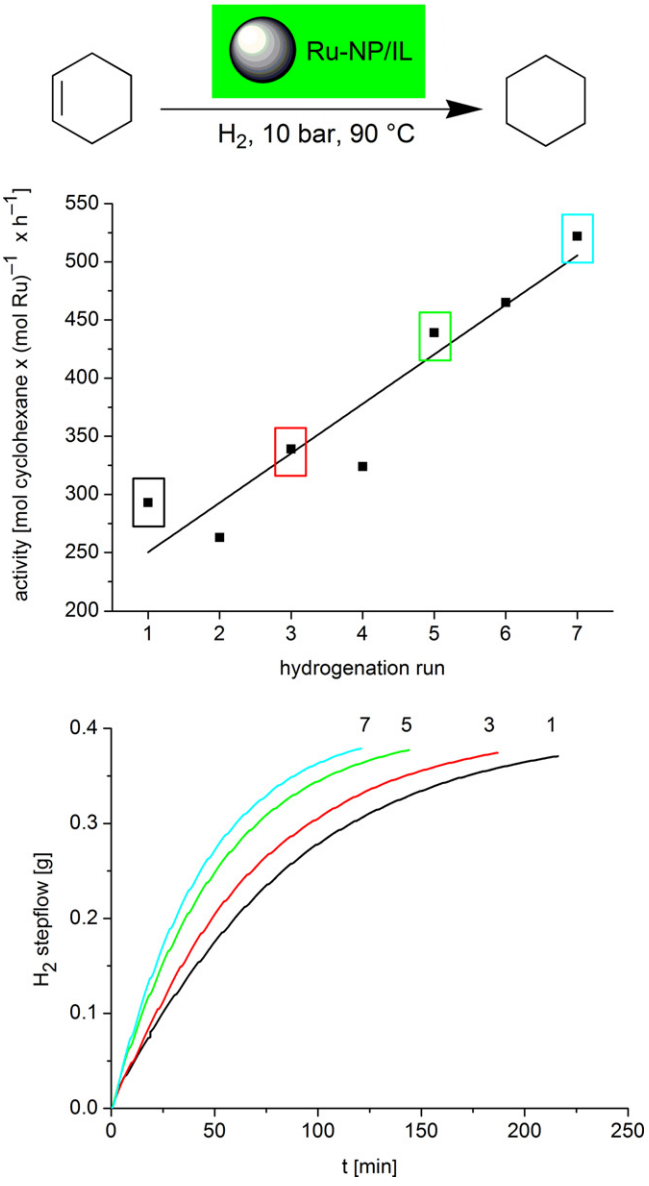

Fig. 11. Activity for seven runs of the hydrogenation of cyclohexene with the same Ru-NP/BMIm$^+$BF$_4^-$ catalyst at 90 °C, 10 bar H_2 pressure, run to 95% conversion and H_2 uptake over time for the 1st, 3rd, 5th and 7th hydrogenation run. An H_2 uptake of 0.38 g corresponds to 95% conversion (100% are 0.2 mol or 0.4 g H_2) [21].

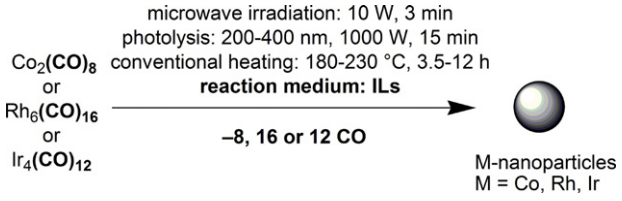

Scheme 10. Formation of Co, Rh and Ir nanoparticles by microwave, photolytic or thermal decomposition of metal carbonyls $M_x(CO)_y$ under argon in ionic liquids [20,21].

380 mol cyclohexane × (mol Rh)$^{-1}$ × h^{-1} for quantitative conversion at 4 bar H_2 pressure and 75 °C (Fig. 14).

Stable ruthenium or rhodium metal nanoparticles could be supported on chemically derived graphene (CDG) surfaces with small and uniform particle sizes (Ru 2.2 ± 0.4 nm and Rh 2.8 ± 0.5 nm) by decomposition of their metal carbonyl precursors $Ru_3(CO)_{12}$ and $Rh_6(CO)_{16}$, respectively, by rapid microwave irradiation in a suspension of CDG in BMIm$^+$BF$_4^-$ (Scheme 11, Fig. 15). The obtained hybrid nanomaterials Rh-NP/CDG and Ru-NP/CDG were – without further treatment – catalytically active in hydrogenation reactions yielding complete conversion of cyclohexene or benzene to cyclohexane under organic-solvent-free and mild conditions (50–75 °C, 4 bar H_2) with reproducible turnover frequencies of 1570 mol cyclohexane × (mol Ru)$^{-1}$ × h^{-1} and 310 mol benzene × (mol Rh)$^{-1}$ × h^{-1}. The catalytically active M-NP/CDG-nanocomposite material could be recycled and used for several runs without any loss of activity. (Scheme 11, Fig. 16) [157].

5. DLVO theory

This section gives a brief overview on the theory for the treatment of particle dispersions.

The classic theory for interaction of two particles in a dispersion is the DLVO (Derjaugin–Landau–Verwey–Overbeek) theory, developed by the research groups of Derjaugin and Landau in the USSR and the group of Vervey and Overbeek in the Netherlands nearly simultaneously in the 1940s. This basic and most commonly theory is considered as a combination of the repulsive Coulomb and the attraction van der Waals forces. Hence DLVO potential is the sum of an effective electrostatic term and a direct van der Waals term.

Some simplifications and assumptions are involved in this theory: the surfaces of the particles are flat. The charge density is homogeneous and remains homogenous, even when particles approach each other. Also there is no change of the concentration of the counter ions which cause the electric potential. The solvent itself has only an influence through its dielectric constant.

It is quite clear that the surface of a particle is not flat and the charge density changes when two particles approach each other. It is evident that the theory can only approximate the real-life interactions of two particles. DLVO theory works very well and is the best predictor of the stability of lyophobic colloids. This theory is fundamental for chemists working on and with colloids [158].

It should be pointed out that there are two main types of stabilizers for NPs: Electrostatic or "DLVO-type" stabilizers which are considered as point charge stabilizers and "classical" steric stabilizers. Small anions like halides seem to be the closest real-life electrostatic stabilizers.

Concerning nanoparticles and their interactions, the anion is the main focus because anions will bind to the unsaturated surface of the electrophilic NP [159]. Thus, the NPs with their anion layer assume a negative charge and turn into a large multi-negative anion. The repulsion between two such negatively charged NPs is the Coulomb part of the DLVO theory.

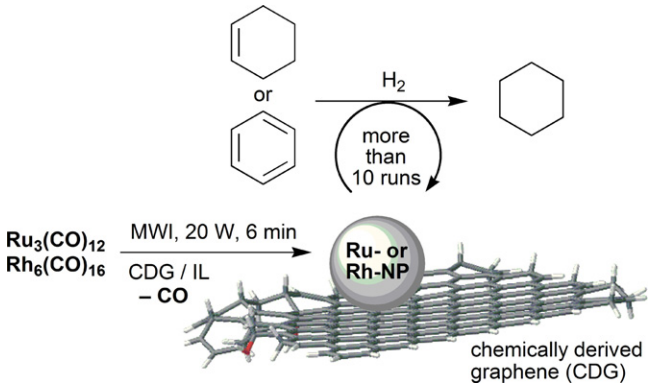

Scheme 11. The use of microwave irradiation for the easy synthesis of transition metal nanoparticles supported on chemically derived graphene (CDG) in ILs. The hybrid nanomaterials Ru-NP/CDG and Rh-NP/CDG were active hydrogenation catalysts [157].

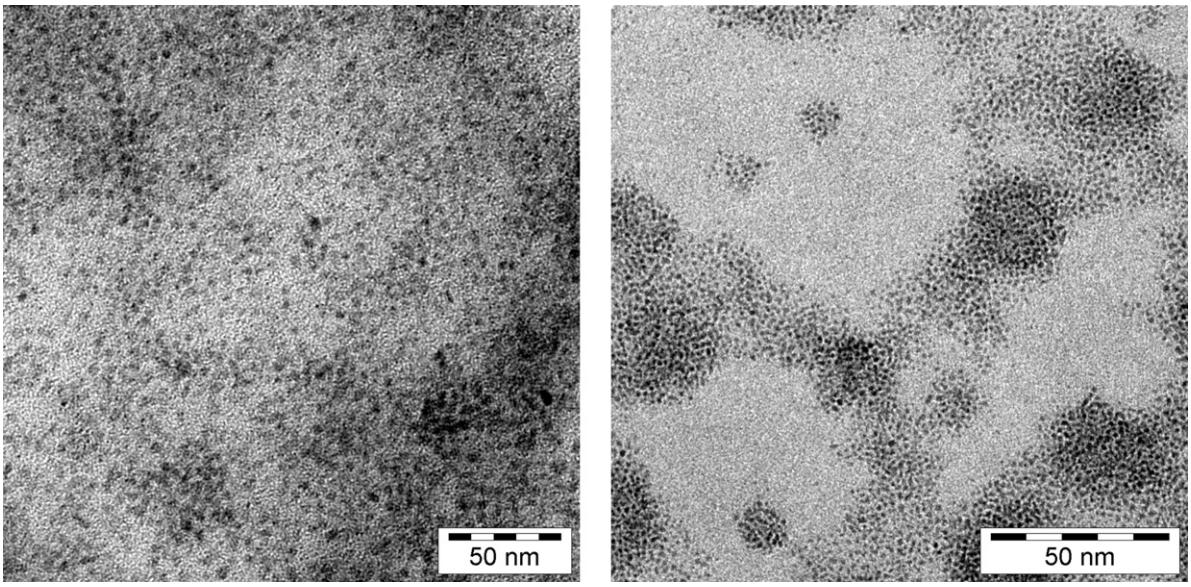

Fig. 12. TEM photographs. Left: Rh-NPs from $Rh_6(CO)_{16}$ (0.5 wt.% Rh in $BMIm^+BF_4^-$, Ø 3.5 (±0.8) nm, entry 10 in Table 4); right: Ir-NPs from $Ir_4(CO)_{12}$ (0.5 wt. % Ir in $BMIm^+BF_4^-$, 18 h, Ø 1.3 (±0.2) nm,, entry 11b in Table 4), both by conventional thermal decomposition [20].

The stability of colloids is a balance between Coulomb forces and van der Waals attraction. A measure of the stability of a colloid is the thickness of the Debye layer, which is the sum of the layers of counterions surrounding the particle. The thicker the Debye layer the more stable is the particle because the distance to the next particle is greater and the van der Waals attraction is reduced. Finke et al. studied the stability of colloids in different solvents and found that the higher the dielectric constant of the medium the better is the stabilization of the colloid [160].

The DLVO theory has its limits. It can only be applied to dilute systems ($<5 \times 10^{-2}$ mol/l). It does not work for higher concentrations. It cannot be applied to ions with multiple charge and sterically stabilized systems [161]. Nowadays the DLVO theory has been supplemented with "extra-DLVO" forces which include effects such as hydrogen bonding, the hydrophobicity and steric interactions.

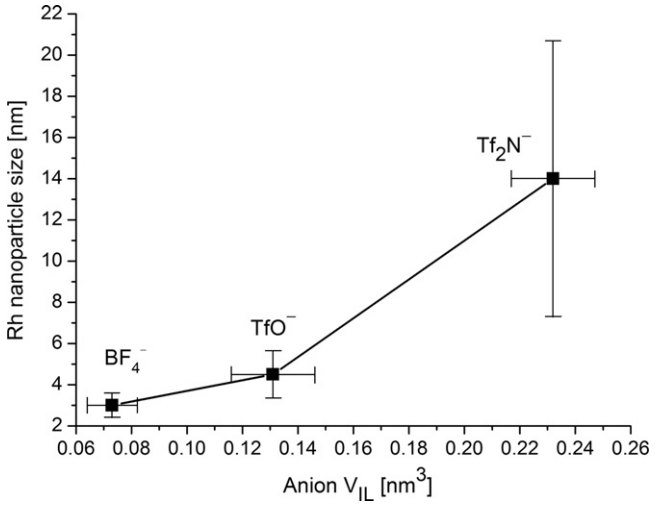

Fig. 13. Correlation between the molecular volume of the ionic liquid anion ($V_{IL\text{-anion}}$) and the observed Rh nanoparticle size with standard deviations as error bars (from TEM). IL anions range from BF_4^- (smallest) over trifluoromethylsulfonate (triflate, $CF_3SO_3^-$, TfO^-) to the largest bis(trifluoromethylsulfonyl)amide [$(CF_3SO_2)_2N^-$, Tf_2N^-] [20].

The van der Waals term is calculated as an integral of interatomic dispersion interactions over the volume of both particles (Eq. (2)) [162].

$$\frac{\mathrm{PMF}^{\mathrm{el}}_{\mathrm{DLVO}}(r)}{k_{\mathrm{b}}T} = L_{\mathrm{B}}Z_1Z_2\frac{\exp(\kappa a_1)\exp(\kappa a_2)}{(1+\kappa a_1)(1+\kappa a_2)}\frac{\exp(-\kappa r)}{r} \quad (2)$$

where PMF is the potential of mean force, L_B the Bjerrum length ($L_B = (e^2/4\pi\varepsilon_r\varepsilon_0)k_bT$), k^{-1} the Debye length, $\kappa^2 = 4\pi L_B\sum_{i=1}^{2}\rho_i Z_i^2$, ρ_i

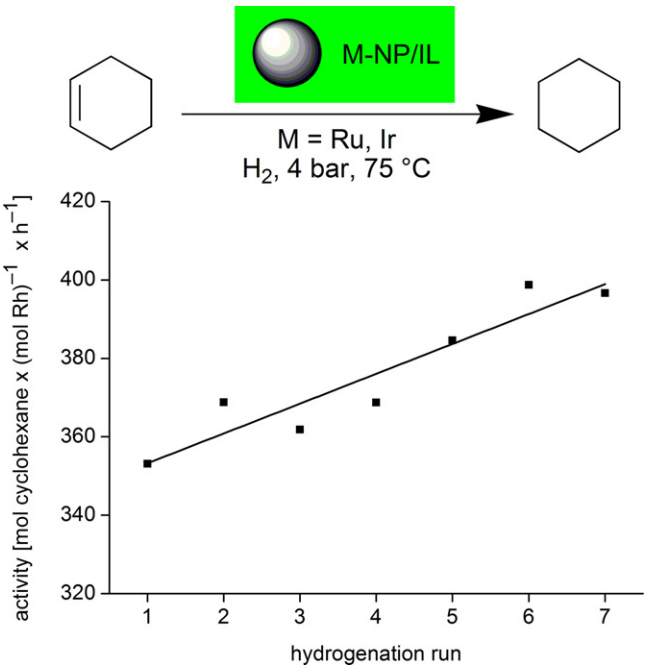

Fig. 14. Activity over seven catalytic runs for the hydrogenation of cyclohexene with the same Rh-NP/$BMIm^+BF_4^-$ catalyst at 75 °C, 4 bar H_2 pressure and 2.5 h reaction time. An activity of 350 mol product × (mol Rh)$^{-1}$ × h^{-1} corresponds to 88% and an activity of 400 to quantitative (100%) conversion. With the homologous Ir-NP/$BMIm^+BF_4^-$ catalyst even higher activities up to 1900 mol cyclohexane × (mol Ir)$^{-1}$ × h^{-1} could be obtained under the same conditions, also due a shorter reaction time of 1 h for near quantitative conversion [20].

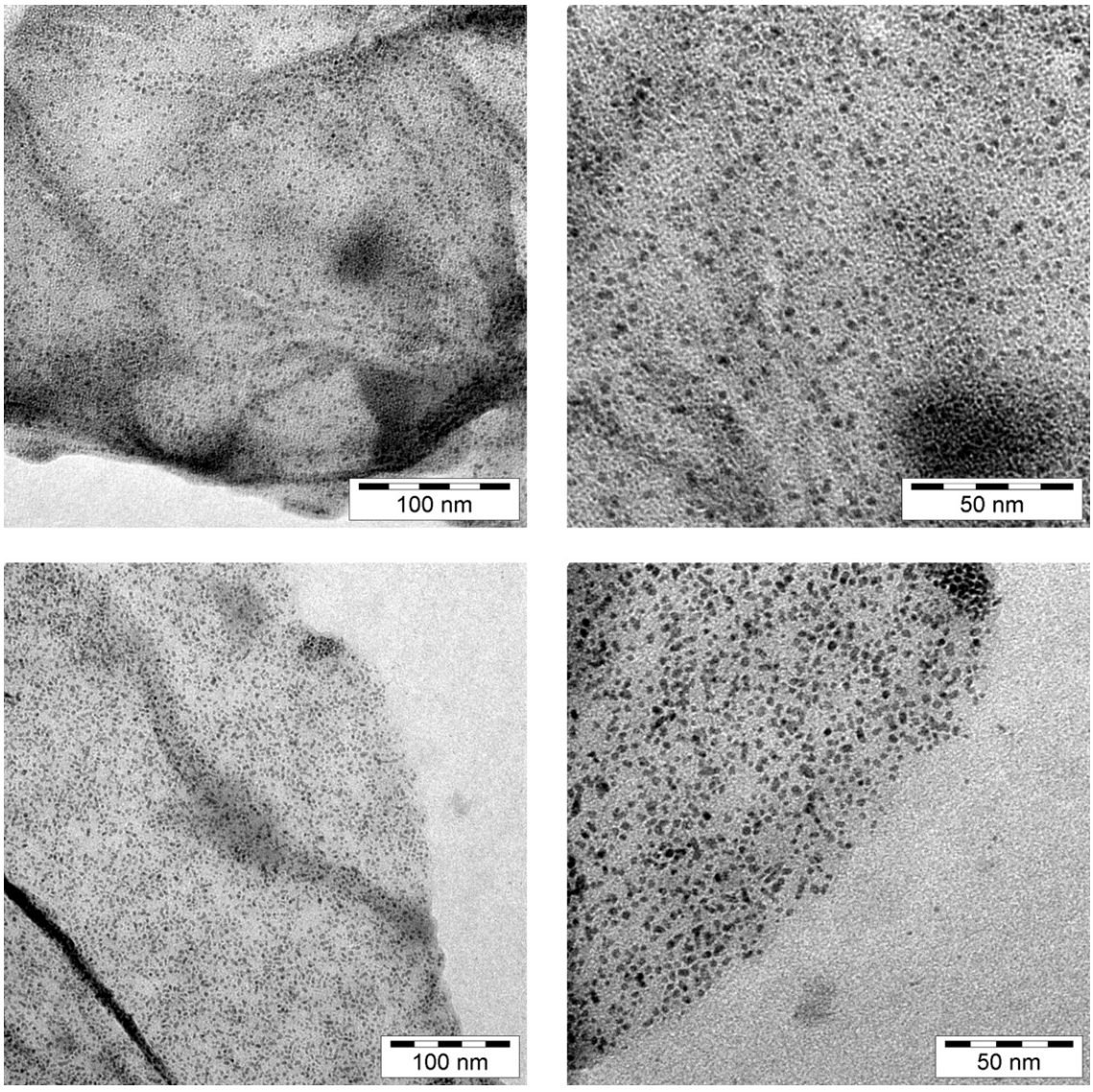

Fig. 15. TEM and TED pictures. Top row: Ru-NP supported on chemically derived graphene (CDG), bottom row: Rh-NP on CDG, from microwave irradiation of $Ru_3(CO)_{12}$ and $Rh_6(CO)_{16}$, respectively, in CDG/$BMIm^+BF_4^-$ [158].

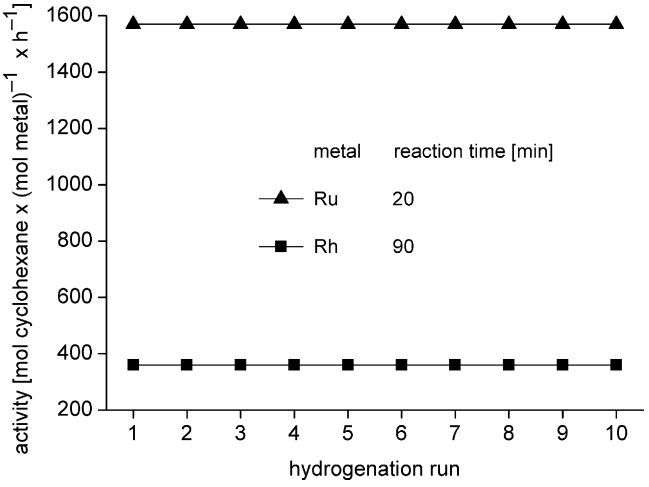

Fig. 16. Activities for the hydrogenation of cyclohexene to cyclohexane with the same M-NP/CDG catalyst in 10 consecutive runs [157].

the concentration of microion i, Z_i the charge of the colloids 1 and 2, a_i the radius of the colloids, and r is the distance between the colloids.

This term is neglected within the basic model, but it is important for large colloidal particles. To compute the effective electrostatic component, microions are described by point charges and two approximations are made, the Poisson–Boltzmann (PB) approximation (that is, a mean-field treatment of micro ions), and an expansion of the charge density to linear order in the electrostatic potential.

Despite its success, the DLVO theory fails to predict some experimental behaviors. The attraction between equally charged particles in the presence of multivalent counterions is the most surprising one [163]. Numerical simulations within the basic model have remarkably contributed to understand such failure. It has been proven that Poisson–Boltzmann theory cannot predict an attraction, while the PMF computed by simulations can be attractive. Therefore, the attraction can be explained by the correlations between microions, missed within the mean field PB treatment, but present in the simulations. The review by Dijkstra devoted to the simulations of charged colloids summarizes work on this issue [163].

6. Conclusions

In this review is shown that ionic liquids (ILs) are remarkable and excellent media for the synthesis and stabilization of metal nanoparticles (M-NPs) without the need of additional stabilizers, surfactants or capping ligands. ILs can be regarded as a supramolecular three-dimensional electrostatic and hydrogen-bonded network. The stabilization of metal nanoparticles in ILs can, thus, be attributed to "extra-DLVO" forces which include effects from the network properties of ILs such as hydrogen bonding, the hydrophobicity and steric interactions to prevent M-NPs agglomeration. Various chemical synthesis methods of metal nanoparticles in ILs allow for the design of a variety of M-NP shapes and sizes. The synthesis of M-NPs can proceed by chemical reduction, thermolysis, photochemical decomposition, electroreduction, microwave and sonochemical irradiation. A microwave induced thermal decomposition of metal carbonyls $M_x(CO)_y$ in ILs provides an especially rapid and energy-saving access to M-NPs because of the ILs significant absorption efficiency for microwave energy due to their high ionic charge, high polarity and high dielectric constant. Metal carbonyls $M_x(CO)_y$ present attractive synthons as they are readily commercially available and contain the metal atoms already in the zero-valent oxidation state needed for M-NPs. No extra reducing agent is necessary and the only side product CO is given off to the gas phase and removed from the dispersion, thereby largely avoiding contaminations of the M-NP/IL dispersion.

Acknowledgments

Our work is supported by the Deutsche Forschungsgemeinschaft through grant Ja466/17-1. We thank the company *IoLiTec* (Germany, www.iolitec.de) for donations of ionic liquids.

References

[1] A.H. Lu, E.L. Salabas, F. Schüth, Angew. Chem. Int. Ed. 46 (2007) 1222; A.H. Lu, E.L. Salabas, F. Schüth, Angew. Chem. 118 (2007) 1242.
[2] A. Gedanken, Ultrasonics Sonochem. 11 (2004) 47.
[3] C.N.R. Rao, S.R.C. Vivekchand, K. Biswas, A. Govindaraj, Dalton Trans. (2007) 3728.
[4] Y. Mastai, A. Gedanken, in: C.N.R. Rao, A. Müller, A.K. Cheetham (Eds.), Chemistry of Nanomaterials, vol. 1, Wiley-VCH, Weinheim, 2004, p. 113.
[5] J. Park, J. Joo, S.G. Kwon, Y. Jang, T. Hyeon, Angew. Chem. Int. Ed. 46 (2007) 4630; J. Park, J. Joo, S.G. Kwon, Y. Jang, T. Hyeon, Angew. Chem. 119 (2007) 4714.
[6] D. Astruc, F. Lu, J.R. Aranzaes, Angew. Chem. Int. Ed. 44 (2005) 7852; D. Astruc, F. Lu, J.R. Aranzaes, Angew. Chem. 117 (2005) 8062.
[7] C. Pan, K. Pelzer, K. Philippot, B. Chaudret, F. Dassenoy, P. Lecante, M.-J. Casanove, J. Am. Chem. Soc. 123 (2001) 7584.
[8] J.D. Aiken III, R.G. Finke, J. Am. Chem. Soc. 121 (1999) 8803.
[9] J. Krämer, E. Redel, R. Thomann, C. Janiak, Organometallics 27 (2008) 1976.
[10] K. Ueno, H. Tokuda, M. Watanabe, Phys. Chem. Chem. Phys. 12 (2010) 1649.
[11] J. Dupont, J.D. Scholten, Chem. Soc. Rev. 39 (2010) 1780.
[12] J. Dupont, J. Brazil. Chem. Soc. 15 (2004) 341.
[13] M.-A. Neouze, J. Mater. Chem. 20 (2010) 9593.
[14] C.S. Consorti, P.A.Z. Suarez, R.F. de Souza, R.A. Burrow, D.H. Farrar, A.J. Lough, W. Loh, L.H.M. da Silva, J. Dupont, J. Phys. Chem. B 109 (2005) 4341.
[15] J. Dupont, P.A.Z. Suarez, R.F. de Souza, R.A. Burrow, J.-P. Kintzinger, Chem. Eur. J. 6 (2000) 2377.
[16] R.A. Sheldon, Chem. Commun. (2008) 3352.
[17] P. Wasserscheid, T. Welton, Ionic Liquid in Synthesis, vol. 1, Wiley-VCH, Weinheim, 2007, pp. 325.
[18] P. Wasserscheid, W. Keim, Angew. Chem. Int. Ed. 39 (112) (2000) 3773; P. Wasserscheid, W. Keim, Angew. Chem. 112 (2000) 3926.
[19] C. van Doorslaer, Y. Schellekens, P. Mertens, K. Binnemanns, D. De Vos, Phys. Chem. Chem. Phys. 12 (2010) 1741.
[20] E. Redel, J. Krämer, R. Thomann, C. Janiak, J. Organomet. Chem. 694 (2009) 1069.
[21] C. Vollmer, E. Redel, K. Abu-Shandi, R. Thomann, H. Manyar, C. Hardacre, C. Janiak, Chem. Eur. J. 16 (2010) 3849.
[22] V. Parvulescu, C. Hardacre, Chem. Rev. 107 (2007) 2615.
[23] D. Astruc, Nanoparticles and Catalysis, Wiley-VCH, New York, 2007.
[24] J. Dupont, R.F. de Souza, P.A.Z. Suarez, Chem. Rev. 102 (2002) 3667.
[25] H. Weingärtner, Angew. Chem. Int. Ed. 47 (2008) 654; H. Weingärtner, Angew. Chem. 120 (2008) 664.
[26] D. Xiao, J.R. Rajian, A. Cady, S. Li, R.A. Bartsch, E.L. Quitevis, J. Phys. Chem. B 111 (2007) 4669.
[27] I. Krossing, J.M. Slattery, C. Daguenet, P.J. Dyson, A. Oleinikova, H. Weingärtner, J. Am. Chem. Soc. 128 (2006) 13427.
[28] K.R. Seddon, Chem. Soc. Rev. 37 (2008) 123.
[29] P. Bonhôte, A.-P. Dias, N. Papageorgiou, K.K. Kalyanasundaram, M. Grätzel, Inorg. Chem. 35 (1996) 1168.
[30] J.M. Pringle, J. Golding, K. Baranyai, C.M. Forsyth, B.B. Deacon, J.L. Scott, D.R. Mc Farelane, New J. Chem. 27 (2003) 1504.
[31] T.J. Gannon, G. Law, R.P. Watson, A.J. Carmichael, K.R. Seddon, Langmuir 15 (1999) 8429.
[32] J.N.A. Canongia Lopes, M.F.C. Gomes, A.A.H. Pádua, J. Phys. Chem. B 110 (2006) 16816.
[33] G. Law, R.P. Watson, A.J. Carmichael, K.R. Seddon, Phys. Chem. Chem. Phys. 3 (2001) 2879.
[34] J.N.A. Canongia Lopes, A.A.H. Pádua, J. Phys. Chem. B 110 (2006) 3330.
[35] D.G.E. Kerfoot, X. Nickel, E. Wildermuth, H. Stark, G. Friedrich, F.L. Ebenhöch, B. Kühborth, J. Silver, R. Rituper, in: Ullmann's Encyclopaedia of Industrial Chemistry, 5th ed., Wiley (online), 2008.
[36] T. Hyeon, Chem. Commun. (2003) 927.
[37] P.H. Hess, P.H. Parker Jr., J. Appl. Polym. Sci. 10 (1966) 1915.
[38] J.R. Thomas, J. Appl. Phys. 37 (1966) 2914.
[39] E. Papirer, P. Horny, H. Balard, R. Anthore, C. Petipas, A. Martinet, J. Colloid Interface Sci. 94 (1983) 207.
[40] E. Papirer, P. Horny, H. Balard, R. Anthore, C. Petipas, A. Martinet, J. Colloid Interface Sci. 94 (1983) 220.
[41] G.H. Lee, S.H. Huh, H.I. Jung, J. Mol. Struct. 400 (1998) 141.
[42] M. Giersig, M. Hilgendorff, J. Phys. D: Appl. Phys. 32 (1999) L111–L113.
[43] U. Wiedwald, M. Spasova, E.L. Salabas, M. Ulmeanu, M. Farle, Z. Frait, A. Fraile Rodriguez, D. Arvanitis, N.S. Sobal, M. Hilgendorff, M. Giersig, Phys. Rev. B 68 (2003) 064424.
[44] J. van Wonterghem, S. Mørup, S.W. Charles, S. Wells, J. Villadsen, Phys. Rev. Lett. 55 (1985) 410.
[45] J. van Wonterghem, S. Mørup, S.W. Charles, S. Wells, J. Colloid Interface Sci. 121 (1988) 558.
[46] C. Pathmamanoharan, N.L. Zuiverloon, A.P. Philipse, Progr. Colloid Polym. Sci. 115 (2000) 141.
[47] A. Goossens, L.J. de Jongh, K. Butter, A.P. Philipse, M.W.J. Crajé, A.M. van der Kraan, Hyperfine Interact. 141–142 (2002) 381.
[48] K. Butter, P.H.H. Bomans, P.M. Frederik, G.J. Vroege, A.P. Philipse, Nat. Mater. 2 (2003) 88.
[49] E. Bauer-Grosse, G. Le Caër, Phil. Mag. B 56 (1987) 485.
[50] S.H. Huh, S.J. Oh, Y.N. Kim, G.H. Lee, Rev. Sci. Instrum. 70 (1999) 4366.
[51] S. Sun, C.B. Murray, D. Weller, L. Folks, A. Moser, Science 287 (2000) 1989.
[52] M. Chen, D.E. Nikles, J. Appl. Phys. 91 (2002) 8477.
[53] M. Chen, D.E. Nikles, Nano Lett. 2 (2002) 211.
[54] V.F. Puntes, K.M. Krishnan, P. Alivisatos, Appl. Phys. Lett. 78 (2001) 2187.
[55] T. Hyeon, S.S. Lee, J. Park, Y. Chung, H.B. Na, J. Am. Chem. Soc. 123 (2001) 12798.
[56] S.-W. Kim, S.U. Son, S.S. Lee, T. Hyeon, Y.K. Chung, Chem. Commun. (2001) 2212.
[57] N.A.D. Burke, H.D.H. Stöver, F.P. Dawson, Chem. Mater. 14 (2002) 4752.
[58] M. Rutnakornpituk, M.S. Thompson, L.A. Harris, K.E. Farmer, A.R. Esker, J.S. Riffle, J. Connolly, T.G. St. Pierre, Polymer 43 (2002) 2337.
[59] F.S. Diana, S.-H. Lee, P.M. Petroff, E.J. Krämer, Nano Lett. 3 (2003) 891.
[60] H. Bönnemann, W. Brijoux, R. Brinkmann, N. Matoussevitch, H. Waldöfner, N. Palina, H. Modrow, Inorg. Chim. Acta 350 (2003) 617.
[61] H. Bönnemann, R.A. Brand, W. Brijoux, H.-W. Hofstadt, M. Frerichs, V. Kempter, W. Maus-Friedrichs, N. Matoussevitch, K.S. Nagabhushana, F. Voigts, V. Caps, Appl. Organomet. Chem. 19 (2005) 790.
[62] S. Behrens, H. Bönnemann, N. Matoussevitch, A. Gorschinski, E. Dinjus, W. Habicht, J. Bolle, S. Zinoveva, N. Palina, J. Hormes, H. Modrow, S. Bahr, V. Kempter, J. Phys.: Condens. Matter 18 (2006) S2543–S2561.
[63] N. Matoussevitch, A. Gorschinski, W. Habicht, J. Bolle, E. Dinjus, H. Bönnemann, S. Behrens, J. Magn. Magn. Mater. 311 (2007) 92.
[64] Y. Yin, R.M. Rioux, C.K. Erdonmez, S. Hughes, G.A. Somorjai, A.P. Alivisatos, Science 304 (2004) 711.
[65] M. Zubris, R.B. King, H. Garmestani, R. Tannenbaum, J. Mater. Chem. 15 (2005) 1277.
[66] B.D. Korth, P. Keng, I. Shim, S.E. Bowles, C. Tang, T. Kowalewski, K.W. Nebesny, J. Pyun, J. Am. Chem. Soc. 128 (2006) 6562.
[67] R.A. Mercuri, PCT Int. Appl. (2007), WO 2007136389, Chem. Abstr. 148 (2007) 37461.
[68] R.A. Mercuri, U.S. Pat. Appl. Publ. (2007), US 2007034050, Chem. Abstr. 146 (2007) 233646.
[69] J.S. Gergely, E.S. Marston, S. Subramoney, L. Zhang, U.S. Pat. Appl. Publ. (2007), US 2007085053, Chem. Abstr. 146 (2007) 433242.
[70] C. Gürler, M. Feyen, S. Behrens, N. Matoussevitch, A.M. Schmidt, Polymer 49 (2008) 2211.
[71] N. Doan, K. Kontturi, C. Johans, J. Colloid Interface Sci. 350 (2010) 126.
[72] L.E.M. Howard, H.L. Nguyen, S.R. Giblin, B.K. Tanner, I. Terry, A.K. Hughes, J.S.O. Evans, J. Am. Chem. Soc. 127 (2005) 10140.
[73] R.D. Rutledge, W.H. Morris III, M.S. Wellons, Z. Gai, J. Shen, J. Bentley, J.E. Wittig, C.M. Lukehart, J. Am. Chem. Soc. 128 (2006) 14210.
[74] I. Robinson, S. Zacchini, L.D. Tung, S. Maenosono, N.T.K. Thanh, Chem. Mater. 21 (2009) 3021.

[75] K.S. Suslick, M. Fang, T. Hyeon, J. Am. Chem. Soc. 118 (1996) 11960.
[76] S.-J. Park, S. Kim, S. Lee, Z.G. Khim, K. Char, T. Hyeon, J. Am. Chem. Soc. 122 (2000) 8581.
[77] K. Butter, A.P. Philipse, G.J. Vroege, J. Magn. Magn. Mater. 252 (2002) 1.
[78] O.A. Platonova, L.M. Bronstein, S.P. Solodovnikov, I.M. Yanovskaya, E.S. Obolonkova, P.M. Valetsky, E. Wenz, M. Antonietti, Colloid Polym. Sci. 275 (1997) 426.
[79] D.P. Dinega, M.G. Bawendi, Angew. Chem. Int. Ed. 38 (1999) 1788; D.P. Dinega, M.G. Bawendi, Angew. Chem. 111 (1999) 1906.
[80] J.-I. Park, J. Cheon, J. Am. Chem. Soc. 123 (2001) 5743.
[81] A. Hütten, D. Sudfeld, I. Ennen, G. Reiss, K. Wojczykowski, P. Jutzi, J. Magn. Magn. Mater. 293 (2005) 93.
[82] D. Sudfeld, I. Ennen, A. Hütten, U. Golla-Schindler, H. Jaksch, G. Reiss, D. Meißner, K. Wojczykowski, P. Jutzi, W. Saikaly, G. Thomas, J. Magn. Magn. Mater. 293 (2005) 151.
[83] A. Taubert, Z. Li, Dalton Trans. (2007) 723.
[84] E. Redel, R. Thomann, C. Janiak, Inorg. Chem. 47 (2008) 14.
[85] T. Gutel, J. Garcia-Anton, K. Pelzer, K. Philippot, C.C. Santini, Y. Chauvin, B. Chaudret, J.-M. Basset, J. Mater. Chem. 17 (2007) 3290.
[86] L.S. Ott, R.G. Finke, Inorg. Chem. 45 (2006) 8382.
[87] G.S. Fonseca, A.P. Umpierre, P.F.P. Fichtner, S.R. Teixeira, J. Dupont, Chem. Eur. J. 9 (2003) 3263.
[88] Z. Li, A. Friedrich, A. Taubert, J. Mater. Chem. 18 (2008) 1008.
[89] P. Migowski, D. Zanchet, G. Machado, M.A. Gelesky, S.R. Teixeira, J. Dupont, Phys. Chem. Chem. Phys. 12 (2010) 6826.
[90] P. Migowski, G. Machado, S.R. Teixeira, M.C.M. Alves, J. Morais, A. Traverse, J. Dupont, Phys. Chem. Chem. Phys. 9 (2007) 4814.
[91] M. Ruta, G. Laurenczy, P.J. Dyson, L. Kiwi-Minsker, J. Phys. Chem. C 112 (2008) 17814.
[92] R.R. Deshmukh, R. Rajagopal, K.V. Srinivasan, Chem. Commun. (2001) 1544.
[93] K. Anderson, S.C. Fernández, C. Hardacre, P.C. Marr, Inorg. Chem. Commun. 7 (2004) 73.
[94] J.M. Zhu, Y.H. Shen, A.J. Xie, L.G. Qiu, Q. Zhang, X.Y. Zhang, J. Phys. Chem. C 111 (2007) 7629.
[95] M.A. Firestone, M.L. Dietz, S. Seifert, S. Trasobares, D.J. Miller, N.J. Zaluzec, Small 1 (2005) 754.
[96] K. Peppler, M. Polleth, S. Meiss, M. Rohnke, J.Z. Janek, Phys. Chem. 220 (2006) 1507.
[97] A. Safavi, N. Maleki, F. Tajabadi, E. Farjami, Electrochem. Commun. 9 (2007) 1963.
[98] K. Kim, C. Lang, P.A. Kohl, J. Electrochem. Soc. 152 (2005) E9.
[99] E. Redel, R. Thomann, C. Janiak, Chem. Commun. 15 (2008) 1789.
[100] G. Schmid, Nanoparticles, 2nd ed., Wiley-VCH, Weinheim, 2010, pp. 214.
[101] M. Antonietti, D. Kuang, B. Smarly, Y. Zhou, Angew. Chem. Int. Ed. 43 (2004), pp. 4988; M. Antonietti, D. Kuang, B. Smarly, Y. Zhou, Angew. Chem. 116 (2004) 5096.
[102] F. Endres, M. Bukowski, R. Hempelmann, H. Natter, H. Angew, Chem. Int. Ed. 42 (2003) 3428; F. Endres, M. Bukowski, R. Hempelmann, H. Natter, H. Angew, Angew. Chem. 115 (2003) 3550.
[103] Y.J. Zhu, W.W. Wang, R.J. Qi, X.L. Hu, Angew. Chem. Int. Ed. 43 (2004) 1410; Y.J. Zhu, W.W. Wang, R.J. Qi, X.L. Hu, Angew. Chem. 116 (2004) 1434.
[104] E.T. Silveira, A.P. Umpierre, L.M. Rossi, G. Machado, J. Morais, G.V. Soares, I.J.R. Baumvol, S.R. Teixeira, R.F.P. Fichtner, J. Dupont, Chem. Eur. J. 10 (2004) 3734.
[105] J. Dupont, G.S. Fonseca, A.P. Umpierre, P.F.P. Fichtner, S.R. Teixeira, J. Am. Chem. Soc. 124 (2002) 4228.
[106] C.W. Scheeren, G. Machado, J. Dupont, P.F.P. Fichtner, S.R. Texeira, Inorg. Chem. 42 (2003) 4738.
[107] A.I. Bhatt, A. Mechler, L.L. Martin, A.M. Bond, J. Mater. Chem. 17 (2007) 2241.
[108] H. Itoh, K. Naka, Y. Chujo, J. Am. Chem. Soc. 126 (2004) 3026.
[109] H. Zhang, H. Cui, Langmuir 25 (2009) 2604.
[110] H.S. Schrekker, M.A. Gelesky, M.P. Stracke, C.M.L. Schrekker, G. Machado, S.R. Teixeira, J.C. Rubim, J. Dupont, J. Colloid Interface Sci. 316 (2007) 189.
[111] R.A. Alvarez-Puebla, E. Arceo, P.J.G. Goulet, J.J. Garrido, R.F. Aroca, J. Phys. Chem. B 109 (2005) 3787.
[112] E.J.W.J.T.G Verwey, Overbeek in Theory of the Stability of Lyophobic Colloids, Dover Publications Mineola, New York, 1999, pp. 1.
[113] E. Redel, J. Krämer, R. Thomann, C. Janiak, GIT Labor-Fachzeitschrift 2008, April, 400.
[114] A.N. Shipway, E. Katz, I. Willner, ChemPhysChem 1 (2000) 18.
[115] T. Cassagneau, J.H. Fendler, J. Phys. Chem. B 103 (1999) 1789.
[116] C.D. Keating, K.K. Kovaleski, M.J. Natan, J. Phys. Chem. B 102 (1998) 9404.
[117] M.N. Kobrak, H. Li, Phys. Chem. Chem. Phys. 12 (2010) 1922.
[118] L.S. Ott, R.G. Finke, Coord. Chem. Rev. 251 (2007) 1075.
[119] B.L. Bhargava, S. Balasubramanian, M.L. Klein, Chem. Commun. (2008) 3339.
[120] E. Redel, M. Walter, R. Thomann, C. Vollmer, L. Hussein, H. Scherer, M. Krüger, C. Janiak, Chem. Eur. J. 15 (2009) 10047.
[121] E. Redel, M. Walter, R. Thomann, L. Hussein, M. Krüger, C. Janiak, Chem. Commun. 46 (2010) 1159.
[122] R.G. Pearson, Chemical Hardness. Application from Molecules to Solids, Wiley-VCH, 1997, pp. 1.
[123] T.A. Baker, C.M. Friend, E. Kaxiras, J. Am. Chem. Soc. 130 (2008) 3720.
[124] K.-S. Kim, D. Demberelnyamba, H. Lee, Langmuir 20 (2004) 556.
[125] S. Gao, H. Zhang, X. Wang, W. Mai, C. Peng, L. Ge, Nanotechnology 16 (2005) 1234.
[126] R. Marcilla, D. Mecerreyes, I. Odriozola, J.A. Pomposo, J. Rodriguez, I. Zalakain, I. Mondragon, Nano 2 (2007) 169.
[127] M.A. Gelesky, A.P. Umpierre, G. Machado, R.R.B. Correia, W.C. Magno, J. Morais, G. Ebeling, J. Dupont, J. Am. Chem. Soc. 127 (2007) 4588.
[128] G.S. Fonseca, G. Machado, S.R. Teixeira, G.H. Fecher, J. Morais, M.C.M. Alves, J. Dupont, J. Colloid Interface Sci. 301 (2006) 193.
[129] C.W. Scheeren, J.B. Domingos, G. Machado, J. Dupont, J. Phys. Chem. C 112 (2008) 16463.
[130] J. Turkevich, P.C. Stevenson, J. Hillier, Discuss. Faraday Soc. 11 (1951) 55.
[131] H.R. Ryu, L. Sanchez, H.A. Keul, A. Raj, M.R. Bockstaller, Angew. Chem. Int. Ed. 47 (2008) 7639; H.R. Ryu, L. Sanchez, H.A. Keul, A. Raj, M.R. Bockstaller, Angew. Chem. 120 (2008) 7751.
[132] Y. Hatakeyama, S. Takahashi, K. Nishikawa, J. Phys. Chem. C 114 (2010) 11098.
[133] T. Kameyama, Y. Ohno, T. Kurimoto, K.-I. Okazaki, T. Uematsu, S. Kuwabata, T. Torimoto, Phys. Chem. Chem. Phys. 12 (2010) 1804.
[134] T. Suzuki, K.-I. Okazaki, S. Suzuki, T. Shibayama, S. Kuwabata, T. Torimoto, Chem. Mater. 22 (2010) 5209.
[135] K. Richter, A. Birkner, A.-V. Mudring, Angew. Chem. Int. Ed. 49 (2010) 2431; K. Richter, A. Birkner, A.-V. Mudring, Angew. Chem. 122 (2010) 2481.
[136] H. Wender, L.F. de Oliveira, P. Migowski, A.F. Feil, E. Lissner, M.H.G. Prechtl, S.R. Teixeira, J. Dupont, J. Phys. Chem. C 114 (2010) 11764.
[137] M.H.G. Prechtl, J.D. Scholten, J. Dupont, Molecules 15 (2010) 3441.
[138] V. Calo, A. Nacci, A. Monopoli, S. Laera, N. Coffi, J. Org. Chem. 68 (2003) 2929.
[139] L. Xu, W. Chen, J. Xiao, Organometallics 19 (2000) 1123.
[140] J.D. Scholten, G. Ebeling, J. Dupont, Dalton Trans. (2007) 5554.
[141] M. Harada, Y. Kimura, K. Saijo, T. Ogawa, S. Isoda, J. Colloid Interface Sci. 339 (2009) 373.
[142] A. Imanishi, M. Tamura, S. Kuwabata, Chem. Commun. (2009) 1775.
[143] P. Roy, R. Lynch, P. Schmuki, Electrochem. Commun. 11 (2009) 1567.
[144] C. Fu, Y. Kuang, Z. Huang, X. Wang, N. Du, J. Chen, H. Zhou, Chem. Phys. Lett. 499 (2010) 250.
[145] S.Z. El Abedin, F. Endres, Electrochim. Acta 54 (2009) 5673.
[146] L. Yu, H. Sun, J. He, D. Wang, X. Jin, X. Hu, G.Z. Chen, Electrochem. Commun. 9 (2007) 1374.
[147] D. Bogdal, Microwave-Assisted Organic Synthesis, Elsevier, New York, USA, 2006, pp. 47.
[148] A.L. Buchachenko, E.L. Frankevich, Chemical Generation and Reception of Radio- and Microwaves, Wiley-VCH, Weinheim, Germany, 1993, pp. 41.
[149] V.K. Ahluwulia, Alternative Energy Processes in Chemical Synthesis, Alpha Science International Ltd., Oxford, United Kingdom, 2008.
[150] J. Berlan, P. Giboreau, S. Lefeuvre, C. Marchand, Tedrahedron Lett. 32 (1991) 2363.
[151] F. Langa, P. de la Cruz, A. de la Hoz, A. Diaz-Ortiz, E. Diez-Barra, Contemp. Org. Synth. 4 (1997) 373.
[152] L. Perreux, A. Loupy, Tetrahedron 57 (2001) 9199.
[153] A. Stadler, C.O. Kappe, J. Chem. Soc. Perkin Trans. 2 (2000) 1363.
[154] A. Stadler, C.O. Kappe, Eur. J. Org. Chem. (2001) 919.
[155] D.O. Silva, J.D. Scholten, M.A. Gelesky, S.R. Teixeira, A.C.B. Dos Santos, E.F. Souza-Aguiar, J. Dupont, ChemSusChem 1 (2008) 291.
[156] M. Scariot, D.O. Silva, J.D. Scholten, G. Machado, S.R. Teixeira, M.A. Novak, G. Ebeling, J. Dupont, Angew. Chem. Int. Ed. 47 (2008) 9075; M. Scariot, D.O. Silva, J.D. Scholten, G. Machado, S.R. Teixeira, M.A. Novak, G. Ebeling, J. Dupont, Angew. Chem. 120 (2008) 9215.
[157] D. Marquardt, C. Vollmer, R. Thomann, P. Steurer, R. Mülhaupt, E. Redel, C. Janiak, Carbon 49 (2011) 1326.
[158] B.W. Ninham, Adv. Colloid Interface Sci. 83 (1999) 1.
[159] R.G. Finke, in: D.L. Feldheim, C.A. Foss Jr. (Eds.), Metal Nanoparticle: Synthesis, Characterization and Applications, Marcel Dekker, New York, 2002 (Chapter 2).
[160] L.S. Ott, R.G. Finke, Inorg. Chem. 45 (2006) 8283.
[161] M. Boström, D.R.W. Williams, B.W. Ninham, Phys. Rev. Lett. 87 (2001) 168103.
[162] J. Lyklema, Fundamentals of Interface and Colloid Science, Elsevier, Amsterdam, 2005.
[163] M. Dijkstra, Curr. Opin. Colloid Interface Sci. 6 (2001) 372.